Journal of Materials Chemistry B

ROYAL SOCIETY OF CHEMISTRY

PAPER

View Article Online
View Journal | View Issue

Check for updates

Cite this: *J. Mater. Chem. B*, 2024, **12**, 7153

Europium–tannic acid nanocomplexes devised for bone regeneration under oxidative or inflammatory environments†

Daniel Fernández-Villa, [ab] María Rosa Aguilar [ab] and Luis Rojo*[ab]

Received 1st April 2024,
Accepted 15th June 2024

DOI: 10.1039/d4tb00697f

rsc.li/materials-b

Europium ions (Eu^{3+}) are gaining attention in the field of regenerative medicine due to increasing evidence of their osteogenic properties. However, inflammatory and oxidative environments present in many bone diseases, such as osteoporosis or rheumatoid arthritis, are known to hinder this regenerative process. Herein, we describe a straightforward synthetic procedure to prepare Eu^{3+}–tannic acid nanocomplexes (EuTA NCs) with modulable physicochemical characteristics, as well as antioxidant, anti-inflammatory, and osteogenic properties. EuTA NCs were rationally synthesized to present different contents of Eu^{3+} on their structure to evaluate the effect of the cation on the biological properties of the formulations. In all the cases, EuTA NCs were stable in distilled water at physiological pH, had a highly negative surface charge ($\zeta \approx -25.4$ mV), and controllable size ($80 < D_h < 160$ nm). *In vitro* antioxidant tests revealed that Eu^{3+} complexation did not significantly alter the total radical scavenging activity (RSA) of TA but enhanced its ability to scavenge H_2O_2 and ferrous ions, thus improving its overall antioxidant potential. At the cellular level, EuTA NCs reduced the instantaneous toxicity of high concentrations of free TA, resulting in better antioxidant (13.3% increase of RSA *vs.* TA) and anti-inflammatory responses (17.6% reduction of nitric oxide production *vs.* TA) on cultures of H_2O_2- and LPS-stimulated macrophages, respectively. Furthermore, the short-term treatment of osteoblasts with EuTA NCs was found to increase their alkaline phosphatase activity and their matrix mineralization capacity. Overall, this simple and tunable platform is a potential candidate to promote bone growth in complex environments by simultaneously targeting multiple pathophysiological mechanisms of disease.

1. Introduction

Bone remodeling is a complex and dynamic process that relies on the interplay between various physiological mechanisms, cell types, and extracellular matrix (ECM) components. In healthy individuals, there is a finely regulated balance between bone formation and bone resorption, but in osteopenic diseases, dysregulations lead to a loss of bone mineral density and a higher risk of fractures.[1] Given the aging of the population, it is estimated that the already high prevalence of these bone diseases (*i.e.*, 200 million estimated cases of osteoporosis worldwide) will continue to increase in the coming decades and new therapeutic strategies are in demand.[2] However, therapies envisioned to promote effective bone regeneration under complex environments need to target not only osteogenic pathways but also additional pathophysiological mechanisms underlying the diseases.

In this regard, both oxidative stress (OxS) and inflammation have been described as factors contributing to bone remodeling dysregulation.[3–6] On the one hand, OxS occurs when the levels of reactive species exceed the antioxidant defense system's capacity to neutralize them, damaging both the ECM and intracellular components.[7,8] In the context of osteopenia, several mechanisms have been identified linking OxS and the loss of bone mass, mainly affecting osteoblasts, osteocytes, and the proteoglycans and glycoproteins composing the ECM.[3–6] On the other hand, under chronic inflammation, such as that observed in rheumatoid arthritis or periodontitis, the persistent release of pro-inflammatory cytokines and chemokines leads to the differentiation and overactivation of osteoclasts, promoting bone resorption and the loss of bone mass.[9,10] Furthermore, chronic inflammation and OxS are closely interconnected, interacting, and amplifying each other, leading to a harmful cycle of tissue damage and dysfunction.[8,11,12]

One promising alternative to simultaneously address these challenges is the use of multi-bioactive nanostructured systems

[a] *Instituto de Ciencia y Tecnología de Polímeros (ICTP) CSIC, 28006 Madrid, Spain. E-mail: rojodelolmo@ictp.csic.es; Tel: +34-915-622-900*
[b] *Centro de Investigación Biomédica en Red de Bioingeniería, Biomateriales y Nanomedicina (CIBER-BBN), 28029, Madrid, Spain*

† Electronic supplementary information (ESI) available. See DOI: https://doi.org/10.1039/d4tb00697f

that could be easily delivered *in situ* to specific areas of interest. In this work, tannic acid (TA), a natural-based polyphenol found in plants, was selected to prepare nano-sized vehicles due to its ability to interact with cations in a pH-dependent manner,[13] and its low price and multiple properties, including antioxidant, anti-inflammatory, anti-cancer, and antibacterial ones.[14–16] Moreover, some bone-regenerative effects have also been reported for TA when coating nanotubes and implants, mainly attributed to its ability to sequester bioactive metals such as strontium, zinc, or magnesium.[17–19]

In this regard, the use of bioactive cations for bone tissue engineering is of particular interest because of their high stability, tunability, reduced cost, and non-immunogenicity.[20] However, there are fewer trivalent cations with reported regenerative properties compared to divalent ones. This phenomenon may be attributed to the adverse effects on calcification processes observed *in vitro* for certain trivalent cations such as Al^{3+}, Ga^{3+}, La^{3+}, and Gd^{3+}. These effects are linked to their tendency to react with the oxygen atoms of the phosphate ions forming hydroxyapatite, due to their high positive charge and small radius, which explains their effective anti-calcification behavior.[21] An intriguing approach to incorporating biocompatible trivalent metals and phenolic linkers involves the preparation of metal-phenolic networks (MPNs), which can be synthesized *via* the coordination of phenolic ligands, mainly polyphenols, and trivalent cations such as Gd^{3+}, Rh^{3+}, Ru^{3+}, V^{3+}, or $Fe^{2+/3+}$, among others.[22] These MPNs offer the possibility of encapsulating specific drugs and biologically active organic molecules for drug delivery, and even for cell encapsulation.[23] Furthermore, lanthanide MPNs, such as those prepared with TA and europium(III) (Eu^{3+}), are gaining attention due to their unique properties for multiple biological applications including sensing and bioimaging.[24,25] Recently, Eu^{3+} has gained attention due to research claiming both osteogenic and angiogenic properties, indispensable features for effective bone regeneration. However, those articles studied the effect of Eu^{3+} on already bioactive materials, such as bioglass or hydroxyapatite formulations,[26–31] as surface coatings,[32,33] or a combination of both[34–36] and mainly assessing their osteogenic potential by studying their effects on the osteoblastic differentiation of mesenchymal stem cells. Thus, the exact mechanism of europium's osteogenic effects has not been elucidated yet.

For all these reasons, in this study, nano-sized complexes based on TA and Eu^{3+} have been devised for future intended applications in osteogenic bones with challenging environments *in situ* (*e.g.*, subchondral or intraosseous administrations), whether as a mono- or as a combinational therapy using advanced injectable formulations. The hypothesis behind this approach is that the complexation of europium by tannic acid would allow for the preservation of the potent antioxidant and anti-inflammatory capabilities of the latter without compromising osteogenic processes due to its acidity, while simultaneously promoting them through the action of europium. Moreover, we have rationally designed them to present different contents of Eu^{3+} to further characterize the contribution of this cation to the final regenerative properties of the system. Herein, we described the synthesis and characterization of Eu^{3+}–tannic acid nanocomplexes (EuTA NCs), as well as their biological effects *in vitro*. Evaluation of their anti-inflammatory and antioxidant properties has been carried out in a macrophage cell line (RAW264.7) while the test of its osteogenic potential has been performed in cultures of human osteoblasts. Altogether, the obtained results present EuTA NCs as a potent antioxidant platform where the addition of europium improves TA cytocompatibility, anti-inflammatory, and osteogenic properties, envisioning their potential applicability for bone regeneration purposes under complex conditions where regeneration is hindered.

2. Materials and methods

2.1. Reagents

$EuCl_3{\cdot}6H_2O$ (96.0%) was purchased from TCI; 1 M HEPES Buffer solution (pH 7.3) for molecular biology, alamarBlue® cell viability reagent, Quant-iT™ PicoGreen™ dsDNA Assay kit, T-PER™ tissue protein extraction reagent and ethylenediaminetetraacetic acid (EDTA) disodium salt dihydrate, 99+% were purchased from ThermoFisher Scientific; 33% w/v hydrogen peroxide (H_2O_2) and sodium hydroxide were purchased from Panreac; hydrochloric acid 37% w/v was purchased from VWR Chemicals; 4-nitrophenyl phosphate, disodium salt, and hexahydrate 98+% was purchased from Acros Organics; 2,2-diphenyl-1-picrylhydrazyl (free radical, DPPH, 95%) was purchased from Alfa-Aesar; and tannic acid (TA, M_w = 1701.2 g mol^{-1}), iron(II) chloride tetrahydrate ($FeCl_2$), 4-nitrophenol, Alizarin red S (AzR), cetylpyridinium chloride (CPC), 2′,7′-dichlorofluorescin diacetate (DCFH-DA), Griess reagent (modified), sodium nitrite ($NaNO_2$) β-glycerophosphate disodium salt hydrate, (+)-sodium L-ascorbate and dexamethasone were purchased from Sigma-Aldrich. All chemicals were used as received.

2.2. Synthesis of EuTA NCs

EuTA NCs were prepared *via* an easy, one-step method at r.t. (~22 °C) by mixing $EuCl_3{\cdot}6H_2O$ and TA solutions under intense sonication. A 50 mM HEPES buffer pH 7.3 was selected to carry out the synthesis as this buffer presents a negligible binding constant for metals and the formation of tris-complexes is favored at neutral pH.[13] Precursor solutions of $EuCl_3{\cdot}6H_2O$ and TA were prepared in distilled water and 50 mM HEPES buffer pH 7.3, respectively, and used immediately to avoid the oxidation and hydrolysis of TA. EuTA NCs formed instantaneously when adding $EuCl_3{\cdot}6H_2O$ dropwise to the TA solution (1 mg mL^{-1} final TA concentration in the mixture) under intense sonication (500 W, 38% amplitude) using a VC-505 ultrasonic processor (Sonics). EuTA NCs were then isolated from their suspensions *via* a centrifugation step at 14 500 rpm for 15 min in a Centrifuge MiniSpin® plus (Eppendorf). Next, pellets were further resuspended in distilled water or culture media and sonicated for 30 s to obtain the final EuTA NCs suspensions. When necessary, suspensions were snap-frozen

with liquid N_2 and freeze-dried using a LyoAlfa 6 freeze-drier (Telstar).

EuTA NCs were devised to present increasing Eu : TA complexation ratios (C.R.) by producing complexes with different contents of Eu^{3+}. As previously demonstrated, to obtain a 100% C.R. between TA and a trivalent cation, a Cat^{3+} : TA molar ratio of 10 : 3 must be applied, as, at pH 7.3, TA and Eu^{3+} have 10 and 3 available coordination positions, respectively.[37] Thus, NCs with 100, 75, 50, and 25% C.R.s were prepared by adding 10 : 3, 7.5 : 3, 5 : 3 and 2.5 : 3 Eu^{3+} : TA molar ratios, respectively.

2.3. Characterization of EuTA NCs

2.3.1. Physicochemical characterization of EuTA NCs

Study of the chemical composition of EuTA NCs. The content of TA and Eu^{3+} on EuTA NCs was calculated using an indirect method. After the centrifugation step, supernatants were examined by UV-VIS (λ_{max} = 278 nm) using a UV-VIS NanoDrop One C spectrophotometer (Thermo Scientific) and by emission spectroscopy on an inductively coupled plasma optical emission spectrometer (ICP-OES, PerkinElmer 430DV) to calculate the content of free TA and Eu^{3+}, respectively. In this regard, the contents of TA and Eu^{3+} on EuTA NCs were calculated by subtracting the content of the free species from the total added during the synthesis. Calibration curves were constructed from the absorbance of a solution series prepared with TA and a europium standard solution, 1000 mg L^{-1} Eu in diluted nitric acid from Eu_2O_3 (Merck). These normalized contents were used to calculate the experimental C.R.s (eqn (1)), the reaction yields of different EuTA NCs (eqn (2)), and the concentrations to use throughout the study.

$$\text{Experimental D.C. (\%)} = \left(\frac{\text{Norm} \cdot \left[Eu^{3+}\right]_{\text{pellet}}}{\text{Norm} \cdot [\text{TA}]_{\text{pellet}}}\right) \times 100 \quad (1)$$

$$\text{N.Y. (\%)} = \left(\frac{\text{Norm} \cdot \left[Eu^{3+}\right]_{\text{pellet}} + \text{Norm} \cdot [\text{TA}]_{\text{pellet}}}{\text{Total}[Eu^{3+}] + \text{Total}[\text{TA}]}\right) \times 100 \quad (2)$$

where Norm·$[Eu^{3+}]_{pellet}$ and Norm·$[TA]_{pellet}$ correspond to the normalized content of Eu^{3+} and TA in the pellets after the isolation step, respectively; and N.Y., Total $[Eu^{3+}]$ and Total [TA] correspond to the normalized yield (defined as the ratio, in percentage, of mass of NCs produced calculated by the sum of the masses of TA and Eu^{3+} in the pellets divided by the sum of the masses of TA and Eu^{3+} added to each synthesis), and the masses of Eu^{3+} and TA added to each synthesis, respectively.

Furthermore, the weight attributed to europium in EuTA NCs was also validated using a direct method by analyzing the pellets instead of the supernatant. For this, different known masses of EuTA NCs were weighed and dissolved in 5 mL of concentrated HCl 37%, to ensure the rupture of tris- and bis-complexes, and then diluted to 20 mL with distilled water for the ICP-OES spectroscopic analysis.

Study of the interaction between Eu^{3+} and TA. Fourier-transform infrared spectroscopy (FTIR) was conducted on a PerkinElmer spectrum two spectrophotometer with an attenuated total reflectance (ATR) attachment to study the chemical compositions of freeze-dried EuTA NCs and to compare them to pristine TA and $EuCl_3$. Analyses were performed using 32 scans and a resolution of 4 cm^{-1}. Finally, spectra were smoothed, corrected to ATR, and normalized for drawing conclusions.

Study of the thermal degradation of EuTA NCs. TGA of freeze-dried NCs was performed using TGA Q500 apparatus (TA instruments) under dynamic N_2 at a heating rate of 5 °C min^{-1} from 30 to 700 °C.

Study of the crystallinity of EuTA NCs. XRD was performed to analyze the crystalline composition of freeze-dried EuTA NCs. Analyses were performed on a Bruker D8 Advance instrument working with CuKα radiation ($n\lambda$ = 1.542 Å) at a 0.01 step size and 0.5 s per step. *D*-spacing values were calculated from the Bragg law equation ($n\lambda = 2d{\cdot}\sin(\varphi)$).

Study of the UV-VIS spectroscopic properties of EuTA NCs. UV-VIS spectroscopy was performed on 2 μg mL^{-1} TA solution and EuTA NC suspensions to compare their maximum absorption wavelengths. Measurements were carried out with the aforementioned NanoDrop spectrophotometer and a quartz cuvette. EuTA NCs' spectra were normalized to their highest absorbance value (*i.e.*, $A_{213\,nm}$).

2.3.2. Morphological characterization of EuTA NCs. The morphology of EuTA NCs was assessed by Cryo-TEM and FE-SEM using a Jeol 1230 electron microscope operated at 100 kV and equipped with a Gatan liquid nitrogen specimen holder for cryo-TEM and a Hitachi SU8000 TED, cold-emission FE-SEM microscope, respectively. Highly diluted suspensions of EuTA NCs samples were applied to holey carbon grids (Quantifoil) after glow-discharge and immediately blotted and vitrified using a FEI Vitrobot cryo-plunger. Cryo-TEM images were taken under low dose conditions with a CMOS Tvips TemCam-F416 camera. Regarding FE-SEM preparation, highly diluted suspensions of EuTA NCs were deposited onto 12-mm glass disks and dried at r.t., before their coating with gold : chromium alloy (80 : 20). The particle size of EuTA NCs was estimated by measuring the diameter of multiple ($n > 50$) nanoparticles from FE-SEM micrographs using the measuring tool of ImageJ/FIJI software (version v1.53c).

2.3.3. Hydrodynamic properties: size distribution, stability, and zeta potential. The hydrodynamic properties of EuTA NCs, including particle size distribution, polydispersity, and zeta potential (ζ), were characterized at 25 °C by DLS and laser Doppler electrophoresis using a Malvern Nanosizer NanoZS Instrument. Measurements were performed on isolated EuTA NCs resuspended in distilled water or Dulbecco's modified Eagle's medium (DMEM, pH 7.4) supplemented with 10 vol% of fetal bovine serum (FBS), which was employed in cell culture studies. The hydrodynamic properties of EuTA NCs were also monitored over time by measuring samples prepared under sterile conditions and stored in the dark at 4 °C. In addition, the stability of EuTA NCs at different pH values was evaluated by preparing 10-mL dispersions of EuTA NCs and adding 10 μL drops of 1 M HCl/NaOH to vary

the pH in a controlled manner without affecting the final concentration.

2.4. Evaluation of the antioxidant properties

The total radical scavenging activity (RSA) of EuTA NCs was evaluated using a DPPH assay adapted from previous studies.[38,39] The 1,1-diphenyl-2-picrylhydrazyl reagent was dissolved at 0.127 mM in ethanol 60%. Similarly, EuTA NCs were prepared as previously specified and resuspended in ethanol 60% after the centrifugation step. Serial dilutions of EuTA NCs were performed in the same solvent to evaluate their antioxidant properties at different concentrations. Next, 100 μL DPPH solution was added to 100 μL of EuTA NCs in the dark. The absorbance at 515 nm was monitored every 5 minutes until reaching the steady state using a multi-detection microplate reader synergy HT (BioTek Instruments). The RSA was calculated using eqn (3):

$$\text{RSA}\ (\%) = \left(\frac{A_{\text{DPPH}} - A_{\text{Sample}}}{A_{\text{DPPH}}}\right) \times 100 \qquad (3)$$

where A_{DPPH} and A_{Sample} correspond to the absorbance of the DPPH itself (blank) and the samples to test, respectively. To calculate the antioxidant potency, RSA values after 15 minutes (in the steady state) were employed. To calculate the velocity of the RSA, the assay was performed under different conditions at their corresponding EC_{50} concentrations. In this regard, results were standardized according to the method reported by Sánchez-Moreno *et al.* using EC_{50}, T_{EC50} and antiradical efficiency (AE):[40] EC_{50} values were defined as the concentration of antioxidant needed to obtain 50% of the maximum RSA at the steady state; T_{EC50} values were defined as the time needed to achieve 50% of the maximum RSA at the EC_{50} concentration; and the AE values were defined as the inverse of the product between EC_{50} and T_{EC50}.

Hydrogen peroxide (H_2O_2) scavenging activity was analyzed following the protocol proposed by Pucci *et al.* with slight modifications.[41] Briefly, 2 μL of 33% w/v H_2O_2 was added to 1998 μL of solutions of TA or EuTA NCs at different concentrations in distilled water. Next, the absorbance of H_2O_2 was immediately measured at 230 nm using the aforementioned NanoDrop spectrophotometer and a quartz cuvette. The corresponding blanks were prepared without H_2O_2, while control samples were prepared with distilled water. The percentage of H_2O_2 scavenging was calculated using eqn (4):

$$H_2O_2\ \text{scavenging}\ (\%) = \left(\frac{A_{H_2O_2} - A_{H_2O_2+\text{sample}}}{A_{H_2O_2}}\right) \times 100 \qquad (4)$$

where $A_{H_2O_2+\text{sample}}$ corresponds to the absorbance of the sample containing H_2O_2, and $A_{H_2O_2}$ the absorbance of the control containing H_2O_2, both at 230 nm.

Fe^{2+} chelating activity was determined using the method reported by Dinis *et al.* with some modifications.[42] TA and EuTA NCs were prepared in distilled water and pHs were adjusted to 7.3 using 1 M NaOH when needed. Then, 37.5 μL of 2 mM $FeCl_2$ solution was added to 300 μL of the samples at different concentrations and left to react for 15 min at r.t. in the dark. Next, 150 μL of 5 mM ferrozine was added and the final volume was adjusted to 3 mL with ethanol. The formation of ferrous chelates was spectrophotometrically calculated by measuring the absorbance at 562 nm using the aforementioned NanoDrop One^C spectrophotometer and eqn (5):

$$Fe^{2+}\ \text{chelating ability}\ (\%) = \left(\frac{A_{H_2O} - A_{\text{sample}}}{A_{H_2O}}\right) \times 100 \qquad (5)$$

where A_{sample} and A_{H_2O} correspond to the absorbance at 562 nm of the antioxidant solutions and control, respectively.

2.5. Biological properties of EuTA nanocomplexes

2.5.1. Cell culture. *In vitro* biological tests were performed using fetal RAW264.7 murine macrophages from the European collection of authenticated cell cultures (ECACC) and human osteoblasts (fHOB cells; 406-05f, Cell Applications, Inc.). Cell lines were cultured in tissue culture T-75 flasks (Sarstedt) with their corresponding media in a series 800 DH incubator (Thermo Scientific, Waltham, MA, USA) under a 5 vol% CO_2 atmosphere at 37 °C. DMEM-high glucose enriched with 4.5 g L^{-1} glucose, sodium pyruvate, and sodium bicarbonate (Sigma-Aldrich) supplemented with 10 vol% FBS, 2 vol% L-glutamine, and 1 vol% of a solution of penicillin/streptomycin (P/S) was used to culture RAW264.7 cells, while an all-in-one ready-to-use growth medium (cell applications) was used for fHOB cell experiments unless stated otherwise. Media was renewed every three or four days.

For these studies, $EuCl_3$ and TA precursor solutions were previously filtered using Millex-GP syringe filter units (0.22 μm), and EuTA NCs were prepared under sterile conditions working on a laminar flow cabinet. For over-time experiments, fresh EuTA NCs were prepared and added at every change of the medium.

2.5.2. Evaluation of EuTA NC cytotoxicity on cultures of RAW264.7 and fHOB cells. The cytotoxicity of TA and EuTA NCs was evaluated on the aforementioned cell lines by measuring the cellular metabolic activity after 24-hour treatment using the alamarBlue® reagent. The cells were seeded in sterile 96-well culture plates (Thermo Scientific) at a density of 10^5 cells per mL in 100 μL of medium and cultured overnight to allow cell attachment. Then, cells were exposed to different concentrations of EuTA NCs and incubated for 24 h. After this, media were removed, and the cells were gently rinsed with phosphate buffer saline at pH 7.4 (PBS) to eliminate unpredictable drug interferences with the reagent as previously studied for other antioxidant compounds.[43] Next, 100 μL of an alamarBlue® solution (10% v/v) prepared in phenol red-free DMEM—low glucose (Sigma-Aldrich) was added to each well. Plates were incubated for 3 h at 37 °C and fluorescence was measured at 590 nm after excitation at 560 nm in a synergy HT microplate reader (BioTek Instruments). IC_{50} values were calculated, when possible, fitting the data to a non-linear, sigmoidal 4PL regression model using GraphPad Prism 8.00 software.

2.5.3. Analysis of NO production on cultures of RAW264.7 macrophages. The anti-inflammatory properties of EuTA NCs were evaluated by measuring the NO released from LPS-stimulated macrophages. RAW264.7 cells were seeded in sterile

96-well culture plates at a concentration of 2×10^5 cells per mL in 100 μL of medium and incubated overnight. After this, cells were incubated for 24 h with different doses of EuTA NCs prepared in media containing 1 μg mL^{-1} LPS. Non-LPS-stimulated cultures were run alongside to confirm the cytocompatibility of the doses. After this, supernatants were collected, mixed in a ratio of 1 : 1 v/v with the Griess reagent kit for nitrite determination, and incubated for 15 min at r.t. in the dark. Then, absorbance at 540 nm was measured and the values were interpolated in a calibration curve constructed with known concentrations of $NaNO_2$. In parallel, cell viability was monitored as previously described using alamarBlue® measurements and employed for normalization purposes.

2.5.4. Scavenging of ROS on cultures of H_2O_2-treated RAW264.7 macrophages. To study the prophylactic effect of EuTA NCs against ROS under cell culture conditions, a well-established DCFH-DA staining was performed to quantify and visualize these protective effects.[44] For this, RAW264.7 macrophages were seeded in sterile 96-well culture plates at a density of 2.5×10^5 cells per mL in 100 μL and incubated overnight. After this, cells were incubated for 24 h with different doses of TA/EuTA NCs prepared in DMEM. Next, cells were rinsed twice with PBS and incubated with 100 μL of a PBS solution containing 20 mM DCFH-DA for 30 min to allow its interiorization. Probe excess was washed away by gently rinsing twice with PBS, and a 100 mM H_2O_2 solution in PBS was then added to each well as the oxidative stimulus. Both negative and positive controls were prepared by adding PBS or PBS + 100 mM H_2O_2 to non-treated cultures respectively. After 15 min of incubation, fluorescence was immediately measured at 485/580 nm (ex/em) with the abovementioned multi-plate reader to avoid a loss of sensitivity, and the content of free radicals was normalized attending to that of the positive controls. After that, images were taken with a fluorescence microscope Nikon Eclipse TE2000-S using a 4× low magnification objective to provide representative fields of each condition.

2.5.5. Effect of EuTA NCs on the proliferation rate of fHOBs. The effect of TA and EuTA NCs on the proliferation rate of fHOBs was evaluated by measuring the metabolic activity after continuous treatment at different time points (t = 1, 3, 6, and 9 days). For this assay, cells were seeded in sterile 96-well culture plates at a density of 10^4 cells per mL in 100 μL of medium, to ensure exponential growth, and cultured overnight to allow cell attachment. Cells were then exposed to different concentrations of the samples and incubated for different periods of time. Both media and compounds were renewed every three days. At each experimental time, the metabolic activity of the cells was monitored as explained above for the cytotoxicity assay. Normalization was performed setting the metabolic activity of untreated cells at 1 day to 100%.

2.5.6. Determination of alkaline phosphatase activity on fHOBs cultures. Monitoring the ALP activity of fHOB cells was selected as a marker of early osteoblastic activity. Cells were seeded in sterile 48-well culture plates at a density of 5×10^4 cells per mL in 200 μL of medium and incubated for 24 h to allow cell attachment. Next, fHOBs were incubated with 10 μg mL^{-1} of TA or EuTA NCs prepared in DMEM during different times (t = 1, 3, and 7 days). Both media and compounds were renewed at three days. At each experimental time, cells were rinsed twice with PBS, and cellular proteins were extracted using tissue protein extraction reagent (T-PER™) buffer (Fisher Scientific) supplemented with Halt™ protease inhibitor cocktail 100× (1 : 100 diluted) without EDTA. Protein extraction and subsequent assays were performed on ice to avoid protein degradation. ALP activity was determined following a previously standardized method,[45] and then it was normalized according to the concentration of double-stranded DNA (dsDNA) content calculated using the PicoGreen assay dye and following the manufacturer's instructions for microtitration.

2.5.7. Effect of EuTA NCs on the mineralization degree of osteoid. To assess the effect of TA and EuTA NCs on the matrix mineralization degree, a quantitative AzR staining assay was performed. For this, fHOBs were seeded in 48-well plates at a density of 5×10^4 cells per mL in 200 μL of medium and incubated overnight to allow cell attachment. Then, cells were incubated with 10 μg mL^{-1} of TA or EuTA NCs prepared in an osteogenic medium during different times (t = 7, 14, and 21 days). The osteogenic medium consisted of advanced DMEM/F12 (1×), containing non-essential amino acids and 110 mg L^{-1} sodium pyruvate, and supplemented with 10 vol% FBS, 2 vol% L-glutamine, 1 vol% P/S, 50 μg mL^{-1} sodium ascorbate, 2 mM β-glycerophosphate disodium salt hydrate, and 0.1 μM dexamethasone, and it was used to induce matrix mineralization in fHOB cultures according to the manufacturer's data. Both media and compounds were renewed every three or four days.

At each experimental time, wells were stained with AzR and quantification using the CPC extraction method was performed as previously described.[45] Representative images were obtained under each condition before AzR extraction using an optical microscope Nikon Eclipse TE2000-S. Ca^{2+} concentration in the matrix was calculated using a calibration curve constructed with known concentrations of AzR in CPC buffer.

2.6. Data analysis and statistics

Results were expressed as means ± standard deviations of at least three experiments carried out with multiple replicates. Statistical analyses were performed using GraphPad Prism 8.00 software. To evaluate differences among groups, the homogeneity of variances was first confirmed and then one-way ANOVA tests, followed by a *post hoc* Scheffe test, were performed. In all the cases, $p < 0.05$ was established to be considered as statistically significant. The results were fitted when necessary to the most appropriate regression models using GraphPad Prism 8.00 software and the parameters are detailed in the ESI.†

3. Results and discussion

In this work, the synthesis of EuTA NCs with different contents of Eu^{3+} in their structures has been reported along with the

characterization of their physicochemical and biological properties, which endorse future preclinical evaluations in *in vivo* models in the context of osteopenic diseases under oxidative and/or inflammatory environments.

3.1. Preparation of EuTA NCs with different contents of Eu^{3+}

There are extensive reports available in the literature on the ability of TA to coordinate trivalent cations, with the ferric one (Fe^{3+}) being the most studied, due to the 10 polyphenolic moieties present in its structure (5 catechols and 5 pyrogallols). In this sense, it has been well-documented that mono-, bis-, and tris-complexes can be formed depending on the pH of the solution.[13]

Considering these data, the preparation of EuTA NCs was carefully devised to retrieve formulations with different contents of europium by adjusting the number of equivalents of $EuCl_3$ added during the synthesis (Fig. 1A), which was confirmed using spectroscopical techniques as shown in Fig. 1B.

Regarding the final products, the normalized yields for the different EuTA NCs increased while augmenting the C.R., as expected (Fig. 1C). This observation can be explained due to the lack of enough Eu^{3+} cations to coordinate all the TA molecules present in the mixture when added in limiting amounts and, therefore, part of the TA added is lost during the preparation. However, differences were also observed when comparing theoretical and experimental C.R. values calculated using ICP-OES. The calculated values were higher than the theoretical ones in all the cases, except for the 100% condition (Fig. 1D). This can be attributed to the high rate of the metal binding reaction with TA. In this sense, in an ideal, homogeneous state, every TA molecule would complex the same amount of Eu^{3+} ions. However, despite the intense sonication during the addition of Eu^{3+}, its complexation was not homogeneous, leading to some TA molecules complexing higher amounts than the calculated average, and others, remaining free in solution, which further agrees with the lower normalized yields calculated experimentally. Thus, the process led to complexes with higher stoichiometry than expected in all the possible cases.

To date, few articles have reported Eu^{3+} complexation by TA, and, to the best of our knowledge, only a couple of them studied regenerative properties.[33,46] Wu *et al.* prepared poly(L-lactic acid) nanofibers coated with different layers of TA/Eu deposits and evaluated the influence of the coating on the physicochemical properties of the material, antioxidant, and wound healing properties.[33] In a later work, Wu *et al.* prepared pH-responsible EuTA microparticles with antioxidant and pro-angiogenic properties for myocardial infarction treatment.[46] Thus, this is the first time that EuTA NCs are reported and studied in depth in the context of oxidative and inflammatory environments that hinder bone regeneration. Moreover, the mechanism of synthesis here proposed is much simpler than those in other works[33,46,47] and allows for easy control of the content of Eu^{3+} present in the formulations by varying the volumes added, which might be of interest to preparing more complex advanced materials in the future.

3.2. Physicochemical characterization of EuTA NCs

The interactions that TA establishes with trivalent cations have been historically studied in-depth and are well-documented, occurring mainly through the hydroxylic groups of its catechol

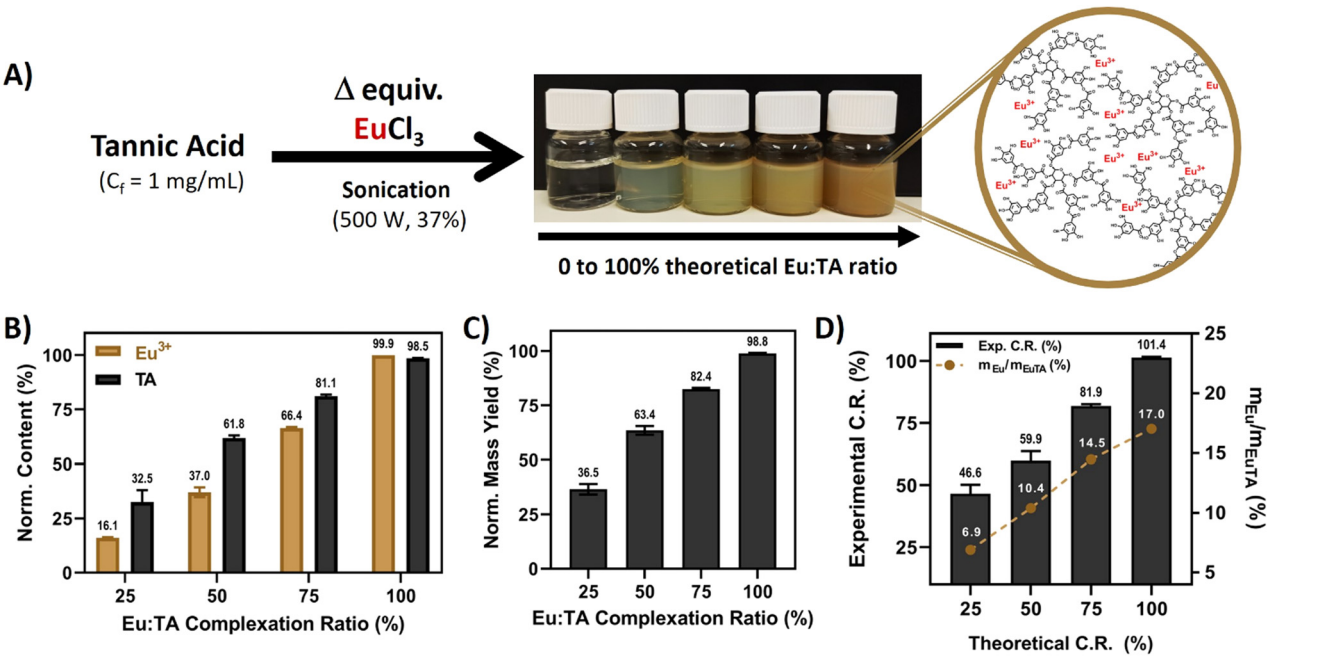

Fig. 1 Synthesis of EuTA NCs and its compositional characterization. (A) Scheme describing the preparation of EuTA NCs and the resulting products; (B) compositional analysis of EuTA NCs as indirectly determined using ICP-OES (Eu^{3+} content) and UV-VIS (TA content) spectroscopies, normalized according to the maximum content of Eu^{3+} and TA added in the synthesis of EuTA 100%; (C) normalized yield of the different EuTA NCs normalized to the maximum theoretical yield; and (D) comparison between experimental and theoretical C.R.s and Eu contribution to weight in each EuTA NC formulation.

structures.[13,48,49] To confirm these interactions, an ATR-FTIR spectroscopic analysis was performed. A zoomed-in region between 400 and 2000 cm^{-1} is shown in Fig. 2A, while the whole spectra and the corresponding frequency assignments

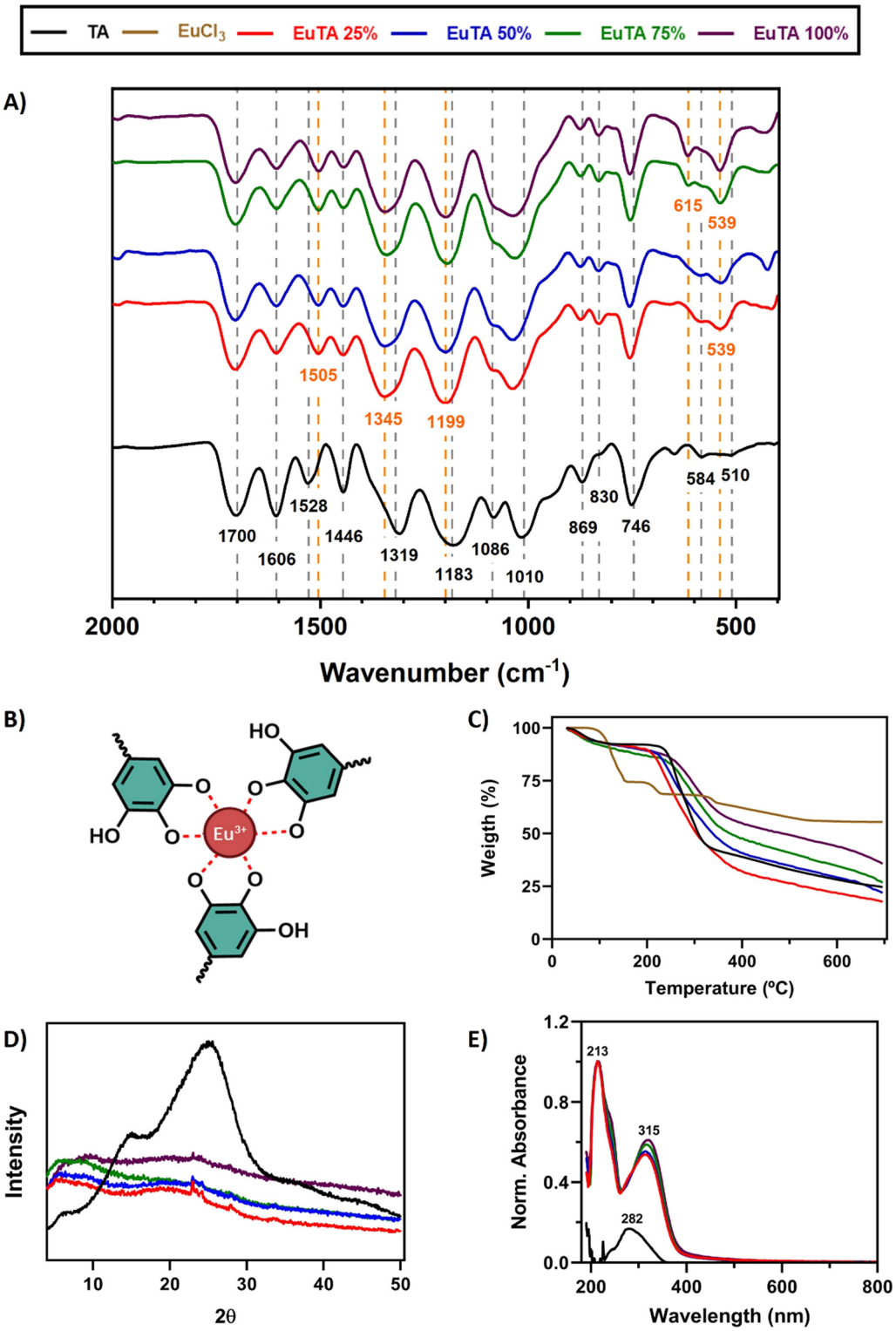

Fig. 2 Characterization of the interaction between TA and Eu^{3+}. (A) Zoomed-in region (2000 and 400 cm^{-1}) of the ATR-FTIR spectra of TA and EuTA NCs; (B) scheme for the tris-complex between Eu^{3+} and the catechol groups (colored) of TA. Black and orange annotated wavenumbers refer to the spectrum of TA and EuTA NCs, respectively; (C) TGA analysis of TA, $EuCl_3$, and EuTA NCs; (D) XRD analysis of TA and EuTA NCs; and (E) UV-VIS spectra of TA and EuTA NCs.

can be found in Fig. S1 and Table S1 (ESI†), respectively. Moreover, the TA structure can be found in Fig. S2 (ESI†). Regarding TA, bands mainly corresponding to the vibrations of aromatic rings, secondary alcohols, and ester groups were identified as expected (Table S1, ESI†), agreeing with previous reports.[48]

A comparison of the spectra of EuTA NCs and raw TA allowed us to conclude that Eu^{3+} complexation exclusively took place *via* hydroxylic groups of the catechol structures, forming tris-complexes (Fig. 2B) as previously described for other trivalent ions.[13,48,49] Briefly, the intensities of three bands (*i.e.*, 1086, ~583, and ~539 cm^{-1}) increased in a directly proportional manner to the content of europium in the NCs. These bands were also present in the FTIR spectrum of the raw $EuCl_3 \cdot 6H_2O$ and corresponded to the stretching and bending ν_{Eu-O}, indicating the participation of oxygen atoms (Fig. S1, ESI†). However, no differences were observed for the stretching vibrations ($\nu_{C=O}$) at 1700 cm^{-1} meaning that the carboxyl groups that form the ester bonds between catechol groups did not participate in europium chelation.[50]

In addition, the stretching vibration ν_{C-O} attributed to the band at 1319 cm^{-1} in the spectrum of TA was the one that shifted the most to higher wavenumbers (~1345 cm^{-1}) after europium complexation, demonstrating the involvement of hydroxyl groups in the chelation. Moreover, the stretching vibrations $\nu_{C=C}$ of the phenol groups also exhibited significant variations. The band located at 1606 cm^{-1} decreased in intensity after europium complexation, while the band at 1528 cm^{-1} increased in intensity and shifted to lower wavenumbers. These two bands have been attributed to the C=C double bonds of the phenolic structures in *ortho*/*para* and *meta* positions, respectively.[51] Similarly, bands attributed to the bending vibrations (ν_{C-H}) in those aromatic structures, such as those at 1183, 869, and 830 cm^{-1}, were also modified, shifting to higher frequencies and altering their intensities, (*i.e.*, decreasing and increasing, respectively). Altogether, europium complexation affected the free mobility of catechol groups through the involvement of their hydroxyl groups. The complexation mechanism between Eu(III) and different tannins has been extensively studied by various authors using a wide range of techniques including potentiometry, calorimetry, XRD, and spectroscopic analysis such as XPS, NMR, and FTIR among others.[46,52–54] These studies have established that during the metal chelation process, the *ortho*-dihydroxyl groups of the catechol ring play a crucial role in facilitating catechol-based coordination with metals. In addition, Arciszewska *et al.* provided an in-depth analysis of the formation mechanisms and molecular structures of Eu-tannin complexes using NMR and FTIR.[54] Their research shows that in Eu(III)/catechol complexes, the hydroxyl groups of the catechol moiety are involved in metal-ion coordination, reducing the hydrogen/electron donating properties of the complex compared to the ligand. Similar conclusions have been drawn for Fe(III)/tannic acid complexes as determined by FTIR. This emphasizes the value of FTIR as a crucial technique for determining the structure of such compounds. FTIR analysis performed on the EuTA NCs corroborates these findings, supporting the notion that metal cation interaction stabilizes the aromatic system forming the tris-complex between Eu^{3+} and the catechol groups proposed in Fig. 2B.

The thermal properties of EuTA NCs were studied by thermogravimetric analysis (TGA, Fig. 2C). The traces of TA and EuTA NCs showed a similar tendency, with two well-defined steps of weight loss. The first decay was found at around 100 °C, which can be attributed to a dehydration step of associated water molecules. The second step of weight loss took place around 220–260 °C and can be assigned to the degradation of TA, as previously reported.[41] In addition, it was found that the remanent weight at 700 °C was dependent on the content of Eu^{3+} in the NCs, confirming once again the different contents of Eu^{3+} in the samples.

The crystallinity of EuTA NCs was studied by X-ray diffraction (XRD) analysis (Fig. 2D and Fig. S3, ESI†). As shown in Fig. 2D, the diffractogram of raw TA showed two wide peaks around 2θ = 15 and 25°, thus, presenting a pronounced amorphous structure due to the great number of hydroxyl groups, which is in accordance with previous reports.[46] In contrast, these characteristic peaks were markedly reduced in the diffractogram of EuTA NCs, as the exposed hydroxyl groups diminished due to the complexation of Eu^{3+}, in accordance with the ATR-FTIR analysis and other works.[46]

Finally, the formation of coordination complexes between TA and Eu^{3+} ions was further confirmed *via* UV-VIS spectroscopy by the appearance of two bands with maximum absorption at 213 and 315 nm, which were not present in the spectrum of TA (Fig. 2E). UV-VIS characterization of a solution of $EuCl_3$ did not retrieve any signal in the range analyzed (data not shown).

3.3. Characterization of the hydrodynamic properties of EuTA NCs

The morphology of EuTA NCs was characterized by different microscopical means. First, EuTA NCs dispersed in culture medium (DMEM) were evaluated by cryo-TEM to assess their morphologies under the conditions selected for the *in vitro* biological testing. As shown in Fig. 3A for EuTA 25% NCs, particles tend to aggregate during sample preparation, hindering the identification of individual particles and the quantification of their mean diameters. Similar results were observed for the rest of the formulations (Fig. S4, ESI†). As an alternative, the morphology of EuTA NCs dried at r.t. was explored by field emission scanning electron microscopy (FE-SEM). In all the cases, pseudospherical nanoparticles were observed, although, similarly to cryo-TEM findings, aggregates formed by the coalescence of these nanoparticles were found in most fields independently of the C.R. values (Fig. S5, ESI†). In contrast, mean diameters of 42.5 ± 9.9 nm averaging all the conditions could be measured. Histograms depicting the different sizes of the nanoparticles are shown in Fig. S6 (ESI†). Thus, as summarized in Fig. 3C and Fig. S5, S6 (ESI†), there were no significant differences in terms of mean nanoparticle size among the studied conditions.

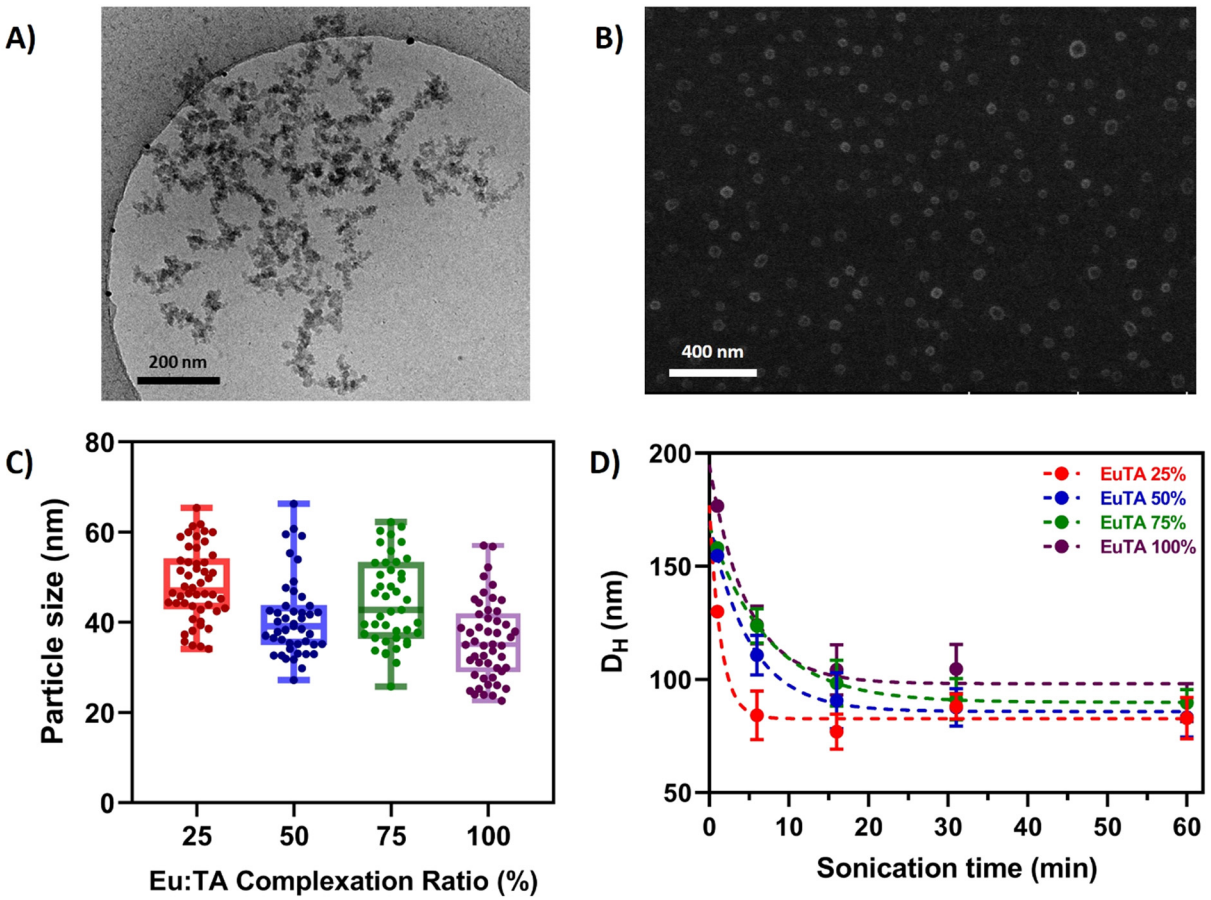

Fig. 3 Physicochemical characterization of EuTA NCs. (A) Cryo-TEM image of EuTA 25% NCs (as a representative image of the different EuTA NCs) in DMEM; (B) FE-SEM micrograph of EuTA 25% NCs (as a representative image of the different EuTA NCs) dried from an aqueous suspension at r.t.; (C) mean particle size of different EuTA NCs calculated from FE-SEM micrographs; and (D) D_h values for EuTA NCs resuspended in distilled water and sonicated during different time periods.

Next, the hydrodynamic properties of the systems were characterized by DLS (Fig. 3D and 4). In all the cases, the average hydrodynamic diameters (D_h) were at least more than twice the mean size reported for individual nanoparticles by FE-SEM. Moreover, increasing the sonication time at the resuspension step diminished the mean D_h values for all the conditions up to 100 nm after 1 hour (Fig. 3D). This finding along with the FE-SEM characterization suggests that nanoparticles tend to form stable nano-sized complexes with different numbers of nanoparticles depending on the duration of the sonication.

In addition, EuTA NCs displayed different hydrodynamic properties depending on the solvent of resuspension. In these studies, distilled water was chosen as a traditional aqueous solvent, while culture medium (DMEM) was selected for its established use in biological cultures. On the one hand, the proposed synthetic procedure retrieved monodispersed (D_h = 150 ± 8 nm) and low-polydispersed (PDI = 0.14 ± 0.02) NCs when resuspended for 30 seconds in distilled water independently of the C.R. (Fig. 4A). In contrast, a strong dependence of D_h and PDI was found with the EuTA composition when resuspended in DMEM, increasing to average values of 222 ± 34 nm and 0.15 ± 0.04, respectively (Fig. 4A). On the other hand, the average zeta potential of EuTA NCs resuspended in distilled water (ζ = −25.4 ± 1.7 mV) rose to −9.5 ± 0.9 mV when resuspended in DMEM (Fig. 4B). These findings can be explained by the ability of serum proteins from DMEM to interact with the TA molecules present at the surface of the EuTA NCs, which are expected to be the determining factor for the negative ζ values obtained. Thus, this interaction would be responsible for the increase of the D_h and the diminishment of the surface net charge.

Regarding the stability of EuTA NCs over time, great differences were observed when comparing EuTA NCs stored in distilled water and DMEM. EuTA NCs stored in distilled water maintained their original hydrodynamic properties to a greater extent than in culture medium (Fig. 4D). In all the cases, increasing the C.R. of the formulations led to higher mean sizes, PDI, and instability over time, specially EuTA 100% NCs. A long-term stability study conducted under these conditions showed similar tendencies although physical degradation of NCs was not found in any case, indicating the suitability of distilled water for long-term storage for up to 2 months (Fig. S7, ESI†). In the case of DMEM-resuspended

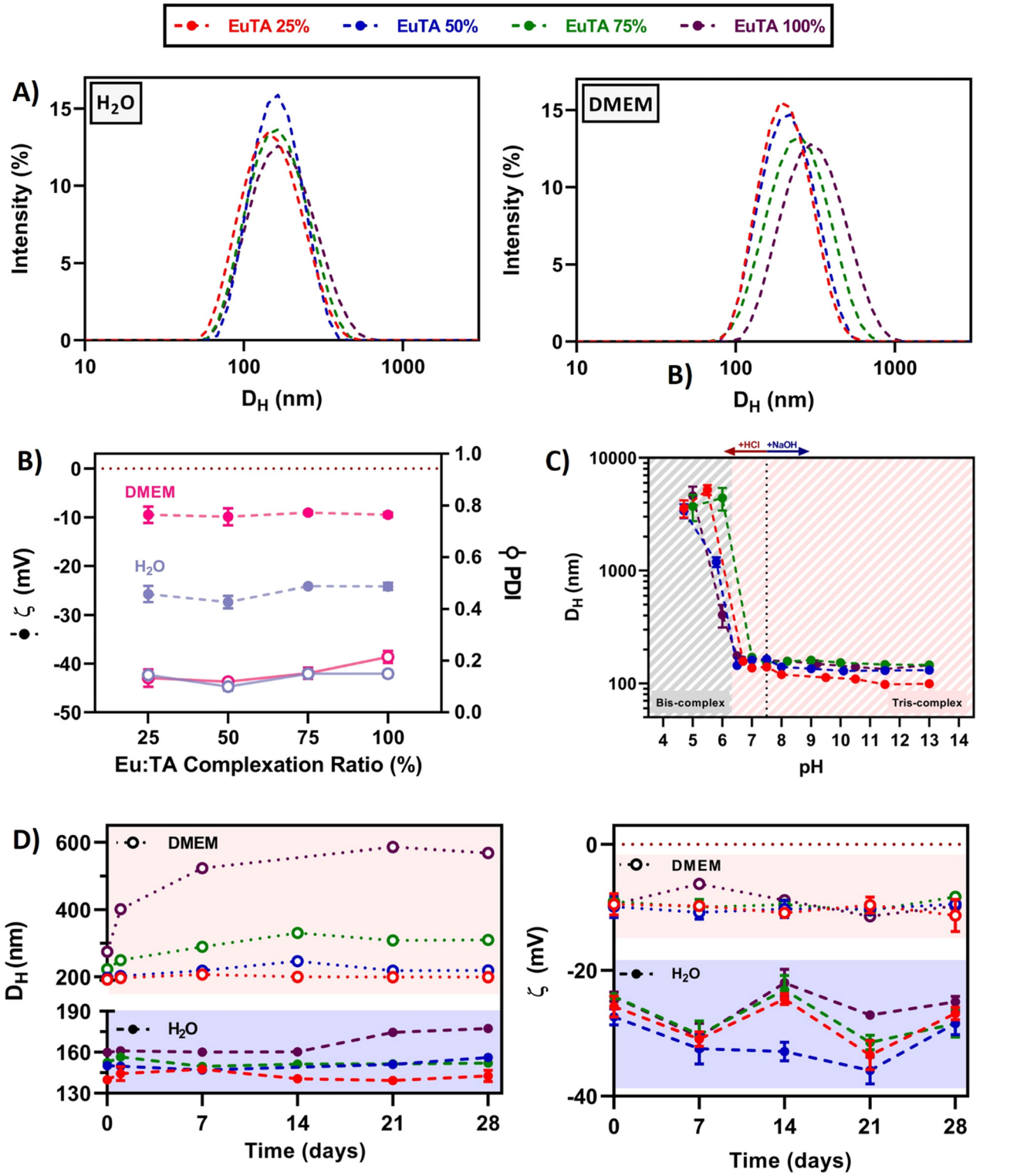

Fig. 4 Hydrodynamic properties of EuTA NCs. (A) Particle size distribution (D_h, by intensity) of EuTA NCs resuspended in distilled water and DMEM; (B) zeta potential (ζ) values and polydispersity index (PDI) of EuTA NCs; (C) stability of EuTA NCs analyzing D_h at different pH values; and (D) stability of EuTA NCs over time including mean D_h and ζ values both in distilled water and DMEM, stored at 4 °C in the dark.

EuTA NCs, the long-term storage mainly affected the conditions with higher C.R. values, where colloidal aggregation was found. Regarding surface net charge, zeta potential values maintained their tendencies over the analyzed month (Fig. 4D). Smaller variations were observed for DMEM-resuspended EuTA NCs compared to the ones resuspended in distilled water, agreeing

with the proposed hypothesis of serum proteins interacting with EuTA NCs.

Furthermore, it was shown that EuTA NCs were stable at neutral and basic pH values (Fig. 4C). However, their conformational structure was distorted below pH 6, leading to the presence of colloidal aggregates. This can be attributed to the type of interactions established between TA and Eu^{3+} ions, as previously studied.[13] In this regard, when reaching values below pH 6, bis-complexes are favored over tris-complexes, and a new reorganization of interactions is arranged, leading to the aggregation of the particles and their precipitation, which is visible to the naked eye. These stability values are acceptable for the intended applications in osteopenic bone as there are some reports of pH measurements performed directly on *in vivo* rat models of osteoporotic bone that confirm a pH of 7.5 for this animal model and disease.[55] In addition, sarcomas and other inflammatory joint diseases, where subchondral bone might be affected, present an increased acidity due to the lack of oxygen in the surroundings. In the case of solid tumors, the pH values range from 6.5–6.8, which would not distort EuTA NC integrity.[56] Although in rheumatoid arthritis-affected joints, synovial cavities can reach values near 6, their possible aggregation would not imply a loss of function of the complexes.[57] Indeed, the previously commented work, carried out by Wu *et al.* on EuTA microparticles, showed the bioactivity of their system despite their large size.[46] However, its controlled delivery by means of advanced injectable formulations is currently under study to avoid any stability concerns and to optimize the bioavailability of the therapy for future intended applications.

3.4. Antioxidant properties of EuTA NCs

The antioxidant activities of TA have been previously reported, being partially attributed to the high redox potential of phenolic groups present in the molecule.[49,58] In this regard, it is important to evaluate the antioxidant properties of EuTA NCs (Fig. 5) due to the partial availability of these groups after the formation of the complexes. To this end, the total radical scavenging activities and, particularly, scavenging activities against H_2O_2 radicals, and ferrous-chelation activities were evaluated. Studying the scavenging of H_2O_2 radicals has biological importance as it is formed under oxidative conditions and leads to cellular damage. Similarly, the Fe^{2+} removal ability is a simple approach to indirectly test the inhibition of lipid peroxidation, as Fe^{2+} ions catalyze Fenton reactions, which produce •OH radicals, resulting in lipid damage.[42] Moreover, it is important to clarify that the concentrations of EuTA NCs commented on from now on (*i.e.*, antioxidant and cell culture experiments) refer to the concentration of TA present in the samples, as calculated by UV-VIS. Thus, at each dose, the amount of TA is constant among conditions while the content of complexed Eu^{3+} is the variable factor.

To compare the total radical scavenging activities of TA and EuTA NCs, a DDPH study was performed. Slight differences were observed in terms of potency (EC_{50}, Fig. 5A and C) and velocity (T_{EC50}, Fig. 5B and C). In all the cases, the kinetics reached plateaus after 10–15 min, ranging the T_{EC50} values between 0.76–1.26 min. Regarding potency, calculated under steady-state conditions, EC_{50} values for TA (4.40 ± 0.09 μg mL^{-1}) and EuTA NCs (4.44 ± 0.62 μg mL^{-1}) were not statistically different from each other. With these values, antiradical efficiencies (AE) were calculated showing a negative trend with the C.R., although in all the cases were found to present "high" or "very high" AE values according to the classification made by Sánchez-Moreno *et al.*[40] A similar behavior has also been reported in nanoparticles of TA complexing Fe^{3+}, which indicates that these changes cannot be attributed to Eu^{3+} itself, but to the coordination with trivalent cations in general.[41] In this sense, our data agree with the hypothesis posed by Pucci *et al.* on the more effective exposure of the reaction sites in free TA compared to coordinated TA, as only T_{EC50}, but not EC_{50}, increased while augmenting the C.R.

In contrast, EuTA NCs showed higher efficacy in the chelation of hydrogen peroxide radicals compared to raw TA. As observed in Fig. 5D, EuTA NC dispersions ($EC_{50} = 46.7 \pm 0.8$ μg mL^{-1}) showed an overall better response than TA ($EC_{50} = 65.3$ μg mL^{-1}), as this effect is independent of the content of Eu^{3+}. Previous reports have associated this effect with a strengthening of the electron-withdrawing capacity of the antioxidant when forming nanosized metal complexes. For instance, NCs of iron–TA and iron–sapogenin showed higher scavenging activities than pure TA and sapogenin, respectively.[59,60] Therefore, this effect would also be dependent on the coordination of these natural-based antioxidants with trivalent cations rather than the individual moieties by themselves. In addition, the oxidation that undergoes TA at physiological pH also influences its scavenging capacity. In this sense, europium complexation seemed to protect TA from its oxidation and hydrolysis at this pH.

In contrast, the ability of EuTA NCs to remove Fe^{2+} did proportionally increase with the content of Eu^{3+} (Fig. 5E). TA removed Fe^{2+} *via* its chelation as previously reported.[61] However, this process is hindered at physiological pH due to the progressive oxidation of TA. Similar to the H_2O_2 scavenging capacity, europium complexation improved this Fe^{2+}-binding capacity, probably by slowing down the oxidation of TA. Nevertheless, in this case, the C.R. of EuTA NCs affected the final response of the system. These differences between assays can be explained by the incubation times of both protocols. In this sense, as the measurements for the determination of the H_2O_2 scavenging were instantaneous, no differences could be observed. In contrast, the ferrozine assay presents a 15-minute incubation time to ensure measurements of the steady state.

Taking these results altogether, the higher removal of H_2O_2 radicals and Fe^{2+} ions would avoid their involvement in Fenton reactions, and indirectly, inhibit lipid peroxidation, protein oxidation, and cell death to a higher extent.[62] Moreover, ferroptosis, a particular type of cell death due to iron overload, has also been reported to be involved in age-related orthopedic diseases such as osteoporosis and osteoarthritis, widening the applicability of these new systems to other bone pathologies.[63] These properties are crucial for reducing OxS, promoting

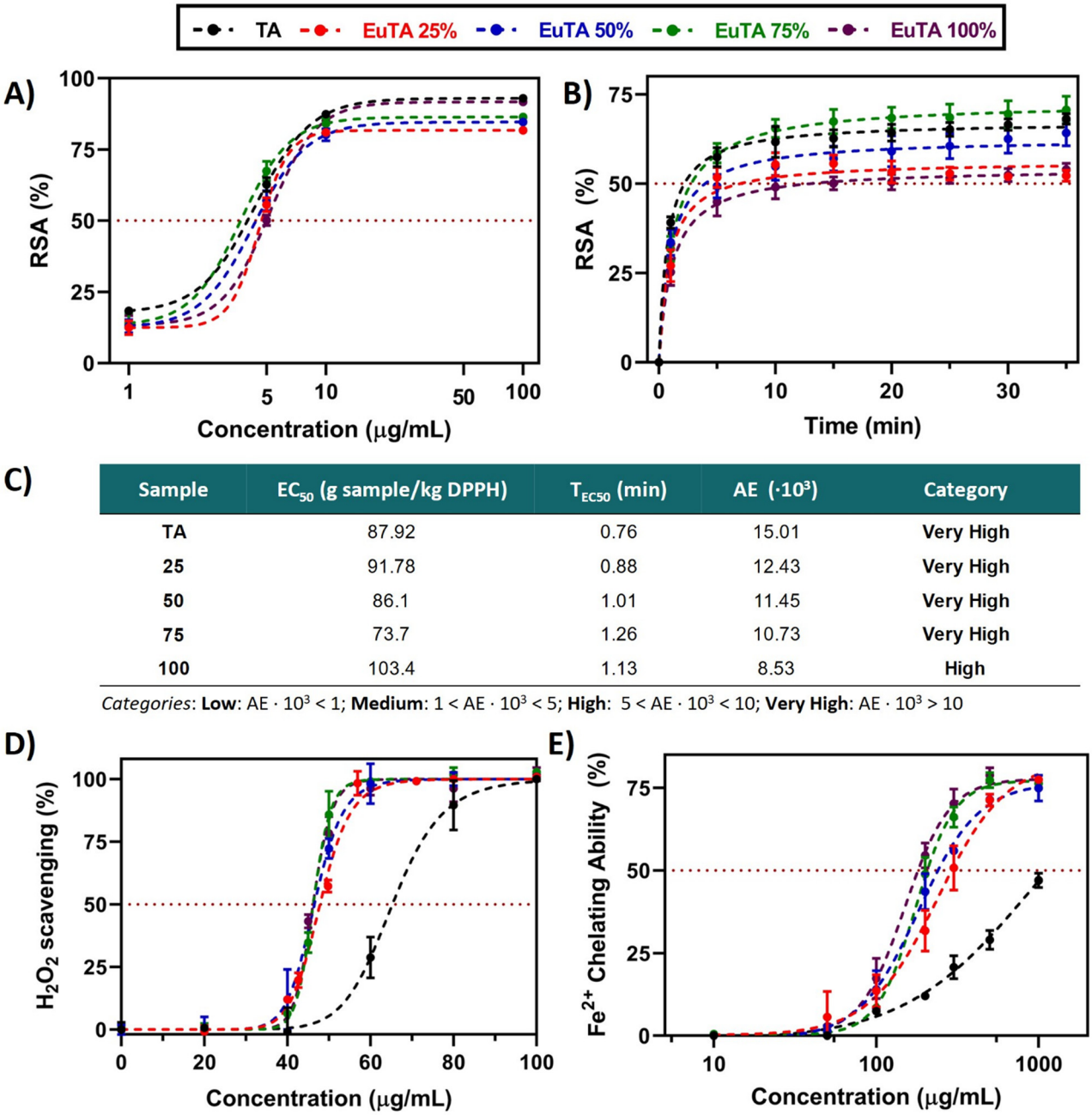

C)

Sample	EC_{50} (g sample/kg DPPH)	T_{EC50} (min)	AE ($\cdot 10^3$)	Category
TA	87.92	0.76	15.01	Very High
25	91.78	0.88	12.43	Very High
50	86.1	1.01	11.45	Very High
75	73.7	1.26	10.73	Very High
100	103.4	1.13	8.53	High

Categories: **Low**: AE · 10^3 < 1; **Medium**: 1 < AE · 10^3 < 5; **High**: 5 < AE · 10^3 < 10; **Very High**: AE · 10^3 > 10

Fig. 5 Antioxidant properties of EuTA NCs. (A) Total free radical scavenging activity (%) of TA and EuTA NCs samples at different concentrations as measured by the DPPH assay at the steady state (15 min), adjusted to a sigmoidal of the variable slope (four parameters) regression model; (B) kinetic of DPPH scavenging by TA and EuTA NCs samples prepared at their corresponding EC_{50}; (C) main parameters for the classification of antioxidants as studied by Sánchez-Moreno *et al.*;[40] (D) H_2O_2 scavenging activity (%) of TA (pH = 7.3) and EuTA NCs at different concentrations, adjusted to [agonist] *vs.* normalized response (variable slope); and (E) ferrous ions chelating ability (%) of TA and EuTA NCs at different concentrations, adjusted to a non-linear (sigmoidal of variable slope) regression model. The parameters for each regression model are summarized in Tables S2–S5 (ESI†).

angiogenesis, and enhancing osteogenesis, all essential processes for bone healing. Research on antioxidant biomaterials for bone regeneration showcases various innovative approaches that compare favorably against traditional methods. Polyphenolic flavonoid silymarin has demonstrated significant antioxidant and anti-inflammatory properties, effectively treating bone fractures and osteoporosis by enhancing ECM secretion and promoting osteogenic markers such as type-I collagen, osteocalcin, and Runx2.[64] Similarly, biodegradable conductive polyphosphazenes have shown strong antioxidant capacity, outperforming conventional polyesters like PLGA by increasing cell viability under high OxS conditions and providing a promising alternative for developing multifunctional scaffolds for severe bone defects.[65] Gelatin hydrogels, integrated with polydopamine nanoparticles and heparin, have demonstrated enhanced bone regeneration capabilities through sustained

BMP-2 release, promoting cell differentiation and mineralization.[66] Finally, other polyphenol-containing materials such as those prepared with TA, including TA–alendronate and Sr-based nano-constructs, have shown promise in promoting osteogenic activity and ROS scavenging. These materials activate signaling pathways such as PI_3K/Akt, fostering bone regeneration and potentially treating osteoporotic defects.[67]

These comparative studies highlight the importance of antioxidant properties in enhancing bone regeneration, with each material offering unique benefits tailored to specific clinical needs. When compared to other antioxidant biomaterials, such as flavonoids, polyphosphazene polymers, gelatin hydrogels, bioactive cation ceramics, and tannic acid complexes, EuTA NCs show unique advantages due to intrinsic dual action where the addition of europium improves TA cytocompatibility, anti-inflammatory, and osteogenic properties, envisioning their potential applicability for bone regeneration purposes under complex conditions where regeneration is hindered.

3.5. Biological characterization of EuTA NCs

EuTA NCs have been devised to target both oxidative and inflammatory environments that hinder bone regeneration. Therefore, their *in vitro* biological characterization must include studies evaluating their cytocompatibility, anti-inflammatory, antioxidant, and osteogenic properties in relevant cellular models.

3.5.1. Anti-inflammatory and antioxidant performance of EuTA NCs in cultures of macrophages. Evaluation of the anti-inflammatory and antioxidant capacities of EuTA NCs was carried out in RAW264.7 macrophages, as this is a widely employed cell line with high secretory potential of pro-inflammatory mediators and ROS in response to specific stimuli.[68]

First, cell viability studies were performed to characterize the possible cytotoxicity of the raw materials and the EuTA NCs after 24 h of incubation in this cell line. As observed in Fig. 6A, both TA and $EuCl_3$ were cytotoxic at high concentrations (IC_{50} = 324.0 μg mL^{-1} and 388.1 μg mL^{-1}, respectively). In contrast, EuTA NCs retrieved viability values over 70% in all the cases (IC_{50} > 1 mg mL^{-1}), confirming their cytocompatibility. We hypothesize that the marked reduction in the cytotoxicity of raw TA after its complexation with Eu^{3+} could be due to the neutralization of their acidic properties, rather than to the presence of europium itself. In this sense, TA was deprotonated during the synthesis when dissolved in HEPES buffer pH 7.3, which allowed the complexation of europium, and after the isolation and resuspension of EuTA NCs, these protons were removed, obtaining neutral pH values in their solutions even in the absence of a pH-buffer.

According to these results, only the effects of cytocompatible doses of each compound were further evaluated in the following tests. In addition, to characterize the contribution of the content of europium, EuTA NCs were compared in all the cases to both an untreated control and TA-treated culture at the same TA concentration.

In many inflammatory diseases, nitric oxide (NO) released by pro-inflammatory macrophages plays a crucial role in the

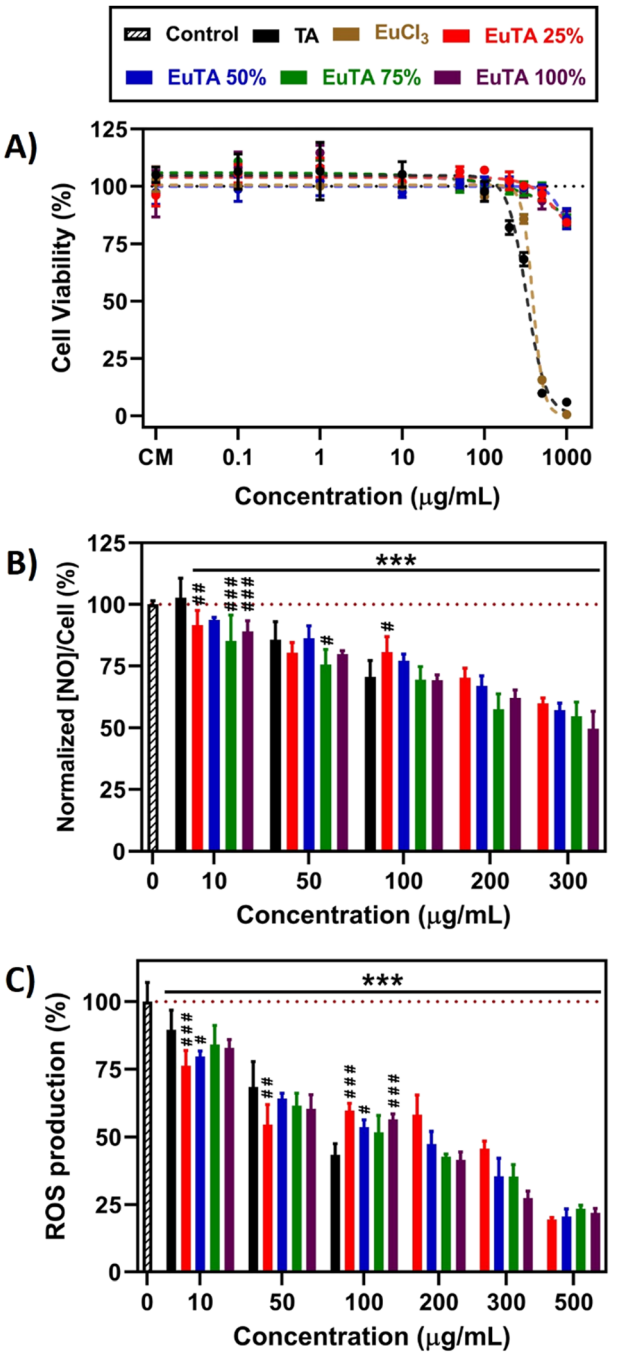

Fig. 6 Antioxidant and anti-inflammatory properties of EuTA NCs evaluated on cultures of RAW264.7 macrophages. (A) Direct cytotoxicity assay following a 24-hour incubation with TA, $EuCl_3$, or the different EuTA NCs and measured using the alamarBlue® method; (B) evaluation of the anti-inflammatory properties of a 24-hour incubation with TA and EuTA NCs assessed by the reduction on the production of NO by LPS-stimulated macrophages and normalized to the metabolic activity of cultures under the same conditions but without LPS-stimulation; (C) evaluation of the ROS scavenging activity of a 24-hour pre-treatment with TA and EuTA NCs before a 15-minute exposure to 100 mM H_2O_2 by measuring the fluorescence of DCFH-DA dye. ANOVA: * and # symbols are used to compare conditions at the same experimental times with control and TA-treated cultures, respectively. Statistical significance: *, # $p < 0.05$; **, ## $p < 0.01$; ***, ### $p < 0.001$.

development and progression of inflammation and, consequently, tissue destruction.[69,70] We examined whether the treatment of LPS-stimulated macrophages with EuTA NCs could reduce the NO secreted, as with TA, which has been previously reported.[71,72] As shown in Fig. 6B, a 24-hour incubation with TA and EuTA NCs diminished this parameter in a concentration-dependent manner. At the lowest dose (10 μg mL^{-1}), TA did not reduce the NO secreted (102.8 ± 7.9%), while EuTA NCs did, and the better performance was from the formulations with higher C.R. values: 75% (85.2 ± 10.5%) and 100% (89.0 ± 4.3%). Analyzing the bigger picture, no statistically significant differences were found among EuTA NCs, although a trend indicating peak performance at 75% C.R. was inferred. Furthermore, NO was reduced too in cultures of resting macrophages, where no LPS was added to stimulate a pro-inflammatory environment (Fig. S8, ESI†). Thus, an improvement in the anti-inflammatory properties of TA has been shown due to Eu^{3+} complexation.

Targeting chronic inflammation is crucial as it can also induce the production of ROS, which can promote the activation of signaling pathways that enhance the production of pro-inflammatory mediators and exacerbate tissue damage.[8,11] Hence, considering the potent antioxidant activities displayed by TA and EuTA NCs against various oxidant agents, we aimed to investigate if subjecting cells to a 24-hour exposure before an oxidant stimulus could offer further preventive effects, potentially reducing future ROS production. In this context, following the initial incubation with the antioxidants, cells were further treated for 15 min with 100 mM H_2O_2, and ROS production was monitored by fluorescence means (Fig. 6C and Fig. S9, ESI†). Similar to the reduction in NO levels, the prophylactic effect of TA and EuTA NCs was concentration-dependent.

Nevertheless, in this case, differences among EuTA NCs did not follow a clear trend. EuTA 75% was the only formulation that did not present significant differences with TA at the same doses. Conversely, at lower concentrations, EuTA 25% displayed a better response, showcasing a 13.3% improvement.

3.5.2. Osteogenic performance of EuTA NCs in cultures of human osteoblasts. Metallic ions have demonstrated promising therapeutic potential in the fields of regenerative medicine and tissue engineering.[73] In particular, divalent metal cations, such as Sr^{2+}, Mg^{2+}, Zn^{2+}, and Cu^{2+}, have been widely utilized to enhance orthopaedic biomaterials following the discovery of their osteogenic effects.[74,75] In contrast, there is currently no trivalent cation therapy in practice. According to the literature, some effects related to bone regeneration have been reported both for TA and Eu^{3+}. On the one hand, TA has been applied as a coating of implants to improve their outcome through several mechanisms such as inhibiting osteoclast differentiation and function, preventing bacterial infections, slowing implants' corrosion, and forming complexes with bioactive trace elements (*e.g.* Ca^{2+}, Sr^{2+}, Mg^{2+}, and Zn^{2+}) that increase osteoblast activity and the overall mineralization degree of the matrix.[19] However, there are not as many reports in the literature on its effects following a soluble administration either *in vitro* or *in vivo in situ*. On the other hand, Eu^{3+} has been used as a doping element in several bioglass and hydroxyapatites to study their osteogenic potential in mesenchymal stem cells as previously commented.[26–31] Thus, there is a gap in existing knowledge regarding the osteogenic potential of TA and Eu^{3+} in the absence of additional osteogenic elements, especially in osteoblast cultures. Accordingly, fHOB cells were selected to evaluate the osteogenic properties of TA and EuTA NCs.

First, cell viability studies were performed analogously to those carried out using RAW264.7 cells. As shown in Fig. 7A, free TA was found to be the most cytotoxic of the studied treatments, presenting an IC_{50} of 107.7 μg mL^{-1}. This finding does not agree with previous works performed in fetal human osteoblasts where an increase in their metabolic activity was reported at increasing concentrations of TA.[76,77] However, these effects might have been overestimated due to the redox potential of TA and the fact that these assays were performed in the presence of the treatments. Therefore, the reduction of the substrate employed for the quantification was due to both the cellular metabolism and TA. In this work, all treatments were removed, and cells were washed with PBS prior to alamarBlue addition to avoid this kind of misinterpretation. Consequently, similar toxicity to that found in RAW264.7 cells was obtained, which could be attributed to the acidity at high doses. In contrast, $EuCl_3$ and EuTA NCs only showed some toxicity at the highest dose assayed, with their IC_{50} values in all cases being over 1 mg mL^{-1}.

Next, we evaluated the effects of cytocompatible concentrations of TA and EuTA NCs on the proliferation rate of fHOBs by monitoring their metabolism. Results obtained for treatments with 10 μg mL^{-1} TA or EuTA NCs are shown in Fig. 7B, while results at lower and higher doses are summarized in Fig. S10 and S11 (ESI†). On the one hand, doses over 10 μg mL^{-1} were shown to impair cell proliferation, although Eu^{3+} complexation diminished to some extent TA toxicity (Fig. S10, ESI†). Moreover, cell vacuolization was observed at higher concentrations on EuTA NCs 50, 75, and 100% after three days of treatment, which we speculate might be due to an excessive supply of Eu^{3+}, as similar reports have been previously reported in cardiomyocytes (Fig. S11, ESI†).[46] On the other hand, while there were no significant differences after short treatments (3 days), longer ones slowed fHOB proliferation depending on the dose. At 0.1 and 1 μg mL^{-1} there were no differences between EuTA NCs and control conditions, but there were if compared to TA (Fig. S10, ESI†). Interestingly, the administration of TA did not increase the metabolic activity of fHOB cells at any assayed dose compared to untreated cultures. In this sense, both TA and its hydrolyzable products (*i.e.*, gallic acid and pyrogallic acid) have been reported to regulate different signaling cascades such as MAPK, PI3K/AKT, or Wnt pathways, although their precise mechanisms of action are still under research.[78,79] However, as commented earlier, other hypotheses consider their metal binding capacities to be pivotal, which would increase the availability of bioactive ions involved in the formation of hydroxyapatite and osteoblast stimulation *in vivo*.[19] Thus, further studies investigating the molecular mechanisms involved in polyphenols' bioactivity are needed to fully comprehend their biomedical potential.

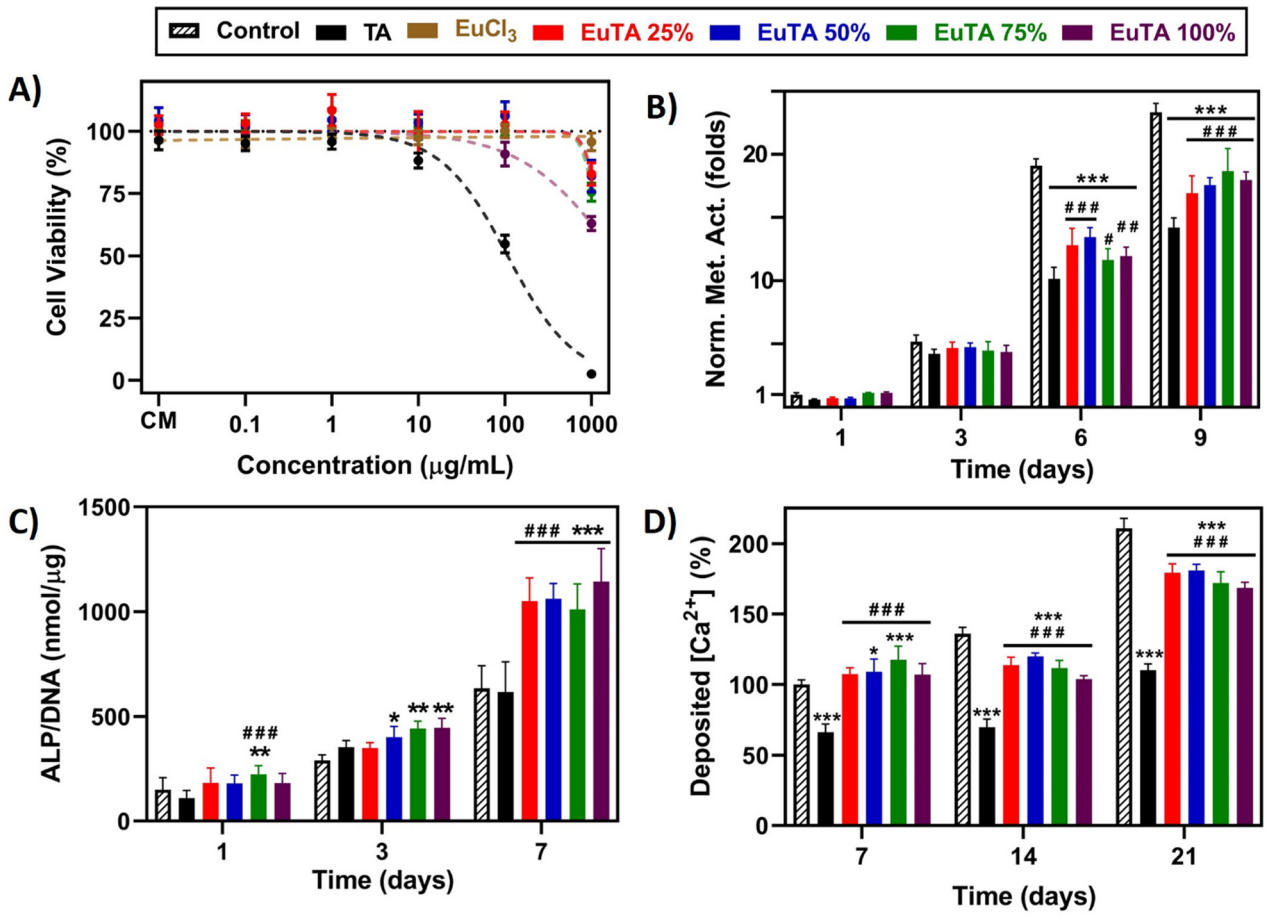

Fig. 7 Osteogenic properties of EuTA NCs evaluated on cultures of fHOBs. (A) Direct cytotoxicity assay following a 24-hour incubation with different concentrations of TA, $EuCl_3$, or the different EuTA NCs and measured using the alamarBlue® method; (B) cell proliferation assay of independent cultures determined by monitoring the metabolic activity *via* alamarBlue® measurements at different incubation times with 10 μg mL^{-1} of TA or EuTA NCs; (C) determination of the ALP activity of cultures treated with 10 μg mL^{-1} of TA or EuTA NCs at different periods of incubation; (D) quantification of AzR staining extracted from cultures treated with 10 μg mL^{-1} of TA or EuTA NCs at different times. ANOVAs: * and # symbols are used to compare conditions at the same experimental times with control and TA-treated cultures, respectively. Statistical significance: *, # $p < 0.05$; **, ## $p < 0.01$; ***, ### $p < 0.001$.

Regarding these proliferation studies, the dose of 10 μg mL^{-1} was selected to study their osteogenic properties, as at that concentration the bioactivity of TA has been proven both throughout this article and in the available literature and it is two orders of magnitude under the IC_{50} values of EuTA NCs.[46] The osteogenic potential of TA and EuTA NCs was assessed at early and late stages by evaluating fHOBs activity, *via* measurements of the alkaline phosphatase (ALP) activity (Fig. 7C), and by analyzing the matrix mineralization degree, *via* alizarin red (AzR) staining (Fig. 7D and Fig. S12, ESI†), respectively.

On the one hand, TA administration did not alter the ALP activity of fHOB cells compared to control cultures at any assayed time (Fig. 7C). However, it significantly diminished the concentration of Ca^{2+} deposited in the ECM, which agrees with its metal-sequestering properties (Fig. 7D). Therefore, the use of TA in solution, rather than in coatings, could be expected to have detrimental effects on bone regeneration applications.

In contrast, EuTA NCs showed a completely different behavior. Regarding ALP activity, small, but statistically significant, differences were observed after one and three days of treatment for the EuTA NCs with higher C.R. values (>25%) (Fig. 7C). However, after 7 days of treatment, ALP values were twice as high as the control and TA-treated cultures for all the formulations. These findings support the evidence of Eu^{3+} having osteogenic properties, as this one of the few reports performed on a healthy, human osteoblast cell line.

Moreover, regarding the effect of EuTA NCs on ECM mineralization, it was found that EuTAs 50 and 75% increased the amount of Ca^{2+} deposited by 9 and 17.5%, respectively, compared to control cultures after 7 days of treatment, thus accelerating the process of ECM maturation (Fig. 7D). In addition, although EuTA 25 and 100% did not significantly alter this parameter at 7 days compared to control cultures, all the formulations showed a better performance than free TA. However, the continuous supply of either TA or EuTA NCs for 14 and 21 days had a negative impact on matrix mineralization. Compared to the control cultures, the addition of the treatments hindered the quantity and the pattern of calcium

deposition, resulting in more localized mineral nodules as opposed to a generalized deposition (Fig. S12, ESI†). Therefore, these results would indicate the use of EuTA NCs for short periods of time to alleviate OxS and inflammation while accelerating the early phases of bone growth. Moreover, evaluating the effect of combinational therapies with more potent osteogenic stimuli such as BMP-2 or BMP-7 could be of interest for maximizing their therapeutic potential.

Taken altogether, this initial study has demonstrated that short-term treatments with 10 μg mL^{-1} EuTA NCs are able to induce osteogenic, antioxidant, and anti-inflammatory effects, outperforming TA in all cases. According to their bioactivity and physicochemical characteristics, EuTA 75% and EuTA 50% were the ones that presented the best overall performances. The mechanisms of action of polyphenols are still under study and, given the lack of visual evidence of their internalization, different hypotheses could be raised including (i) their action occurs at the extracellular level leading to signaling cascades *via* different routes, or (ii) EuTA NCs are dissociated or partially hydrolyzed when entering the cells. Therefore, given their potential and these biological queries to be checked, more complex models using injectable therapies to control their spatiotemporal administration and evaluate the biochemical pathways involved in their effects are currently under study. Moreover, strategies incorporating other bioactive cations that enhance these properties to a greater extent or add novel ones might be a promising research line to exploit in future studies. In this sense, their high stability, low doses needed, and short-term application times are excellent features to provide more complex systems with these bioactive properties.

4. Conclusions

In this study, tunable EuTA NCs with varying Eu^{3+} contents have been developed and characterized for their physicochemical and biological properties in the context of bone regeneration under oxidative and inflammatory conditions. Complexation with Eu^{3+} did not compromise the bioactive properties of TA but enhanced certain antioxidant properties while reducing cellular toxicity. Additionally, EuTA NCs demonstrated superior performance to TA in promoting both early and late markers of osteoblast activity with short-term treatments. Although further research is needed to fully evaluate the regenerative potential of these systems under physiological conditions in *in vivo* models, these *in vitro* studies present EuTA NCs as suitable candidates to be applied *in situ* to resolve OxS and inflammation while promoting early bone regenerative processes.

Author contributions

Daniel Fernández Villa: conceptualization, data curation, formal analysis, investigation, methodology, software, supervision, visualization, writing – original draft, writing – review and editing; María Rosa Aguilar: funding acquisition, investigation, project administration, resources, supervision, visualization, writing – review and editing. Luis Rojo: conceptualization, funding acquisition, investigation, project administration, resources, supervision, visualization, writing – review and editing.

Data availability

Data for this article, will be available at DIGITAL.CSIC, the institutional repository of the Spanish National Research Council.

Conflicts of interest

There are no conflicts to declare.

Acknowledgements

This paper is dedicated to the memory of Blanca Vázquez-Lasa, who participated in the conceptualization and preliminary studies of this work, but lamentably passed away on 31st January 2023. This research has been funded by the Spanish MICINN (PID2020-114086RB-I00) and Comunidad Autónoma de Madrid (S2022/BMD-7406). D. F.-V. is financially supported by a predoctoral program MICINN FPU18/04683. M. R. A. and L. R. are members of PTI-SusPlast+ and Nanomedicine CSIC. The authors would like to acknowledge David Gómez, Pedro González Esperanza Benito and Pilar Posadas of the Characterization Service at the Instituto de Ciencia y Tecnología de Polímeros (CSIC) for the technical support and EM facilities of the CIB Margarita Salas (CSIC) for support in grid screening and preparation.

References

1 J. S. Kenkre and J. H. D. Bassett, *Ann. Clin. Biochem.*, 2018, **55**, 308–327.
2 N. Salari, H. Ghasemi, L. Mohammadi, M. hasan Behzadi, E. Rabieenia, S. Shohaimi and M. Mohammadi, *J. Orthop. Surg. Res.*, 2021, **16**, 609.
3 C. Cervellati, G. Bonaccorsi, E. Cremonini, A. Romani, E. Fila, M. C. Castaldini, S. Ferrazzini, M. Giganti and L. Massari, *Biomed Res. Int.*, 2014, **2014**, 569563.
4 M. Abdollahi, B. Larijani, R. Rahimi and P. Salari, *Therapy*, 2005, **2**, 787–796.
5 T. Iantomasi, C. Romagnoli, G. Palmini, S. Donati, I. Falsetti, F. Miglietta, C. Aurilia, F. Marini, F. Giusti and M. L. Brandi, *Int. J. Mol. Sci.*, 2023, **24**, 3772.
6 M. Chen, Y. Wang, S. Deng, Z. Lian and K. Yu, *Front. Cell Dev. Biol.*, 2022, **10**, 964130.
7 V. Domazetovic, G. Marcucci, T. Iantomasi, M. L. Brandi and M. T. Vincenzini, *Clin. Cases Miner. Bone Metab.*, 2017, **14**, 209–216.
8 J. Gambini and K. Stromsnes, *Biomedicines*, 2022, **10**, 753.
9 H. Newman, Y. V. Shih and S. Varghese, *Biomaterials*, 2021, **277**, 121114.

10 M. A. Terkawi, G. Matsumae, T. Shimizu, D. Takahashi, K. Kadoya and N. Iwasaki, *Int. J. Mol. Sci.*, 2022, **23**, 1786.
11 S. Chatterjee, in *Oxidative Stress and Biomaterials*, ed. T. Dziubla and D. A. Butterfield, Elsevier Inc., 2016, pp. 35–58.
12 L. Kang, H. Zhang, C. Jia, R. Zhang and C. Shen, *Front. Pharmacol.*, 2022, **13**, 956355.
13 S. Çakar and M. Özacar, *J. Photochem. Photobiol., A*, 2019, **371**, 282–291.
14 Z. Guo, W. Xie, J. Lu, X. Guo, J. Xu, W. Xu, Y. Chi, N. Takuya, H. Wu and L. Zhao, *J. Mater. Chem. B*, 2021, **9**, 4098–4110.
15 W. Jing, C. Xiaolan, C. Yu, Q. Feng and Y. Haifeng, *Biomed. Pharmacother.*, 2022, **154**, 113561.
16 A. Bigham, V. Rahimkhoei, P. Abasian, M. Delfi, J. Naderi, M. Ghomi, F. Dabbagh Moghaddam, T. Waqar, Y. Nuri Ertas, S. Sharifi, N. Rabiee, S. Ersoy, A. Maleki, E. Nazarzadeh Zare, E. Sharifi, E. Jabbari, P. Makvandi and A. Akbari, *Chem. Eng. J.*, 2022, **432**, 134146.
17 B. Onat, S. Ozcubukcu, S. Banerjee and I. Erel-Goktepe, *Eur. Polym. J.*, 2018, **103**, 101–115.
18 C. Steffi, Z. Shi, C. H. Kong, S. W. Chong, D. Wang and W. Wang, *Polymers*, 2019, **11**, 1256.
19 Y. Sun, Y. Qu and J. Zhao, *Front. Mater.*, 2022, **8**, 801369.
20 M. Jiménez, C. Abradelo, J. San Román and L. Rojo, *J. Mater. Chem. B*, 2019, **7**, 1974–1985.
21 W. M. Tan, W. K. Loke, B. L. Tan, A. Wee, E. Khor and K. S. Goh, *Biomaterials*, 1993, **14**, 1003–1007.
22 W. Xie, Z. Guo, L. Zhao and Y. Wei, *Theranostics*, 2021, **11**, 6407–6426.
23 G. Fan, J. Cottet, M. R. Rodriguez-Otero, P. Wasuwanich and A. L. Furst, *ACS Appl. Bio Mater.*, 2022, **5**, 4687–4695.
24 W. Zhu, S. Liang, J. Wang, Z. Yang, L. Zhang, T. Yuan, Z. Xu, H. Xu and P. Li, *J. Mater. Sci.: Mater. Med.*, 2017, **28**, 1–11.
25 H. Wang, D. Wang, J. Yu, Y. Zhang and Y. Zhou, *Biomater. Sci.*, 2022, **10**, 5786–5808.
26 G. Miao, X. Chen, C. Mao, X. Li, Y. Li and C. Lin, *J. Sol-Gel Sci. Technol.*, 2014, **69**, 250–259.
27 C. Wu, L. Xia, P. Han, L. Mao, J. Wang, D. Zhai, B. Fang, J. Chang and Y. Xiao, *ACS Appl. Mater. Interfaces*, 2016, **8**, 11342–11354.
28 M. Shi, L. Xia, Z. Chen, F. Lv, H. Zhu, F. Wei, S. Han, J. Chang, Y. Xiao and C. Wu, *Biomaterials*, 2017, **144**, 176–187.
29 Y. Zhang, M. Hu, X. Wang, Z. Zhou and Y. Liu, *Nanomaterials*, 2018, **8**, 961.
30 F. Li, M. Wang, G. Pi and B. Lei, *J. Biomed. Nanotechnol.*, 2018, **14**, 756–764.
31 M. Alicka, P. Sobierajska, K. Kornicka, R. J. Wiglusz and K. Marycz, *Mater. Sci. Eng., C*, 2019, **99**, 1257–1273.
32 R. Augustine, S. K. Nethi, N. Kalarikkal, S. Thomas and C. R. Patra, *J. Mater. Chem. B*, 2017, **5**, 4660–4672.
33 K. Wu, X. Wu, J. Guo, Y. Jiao and C. Zhou, *Adv. Healthcare Mater.*, 2021, **10**, 1–13.
34 M. Sikora, K. Marcinkowska, K. Marycz, R. J. Wiglusz and A. Smieszek, *Materials*, 2019, **12**, 3779.
35 K. Marycz, A. Smieszek, S. Targonska, S. A. Walsh, K. Szustakiewicz and R. J. Wiglusz, *Mater. Sci. Eng., C*, 2020, **110**, 110634.
36 M. Liu, M. Shu, J. Yan, X. Liu, R. Wang, Z. Hou and J. Lin, *Nanoscale*, 2021, **13**, 1181–1194.
37 H. Fan, L. Wang, X. Feng, Y. Bu, D. Wu and Z. Jin, *Macromolecules*, 2017, **50**, 666–676.
38 M. Huerta-Madroñal, J. Caro-León, E. Espinosa-Cano, M. R. Aguilar and B. Vázquez-Lasa, *Carbohydr. Polym.*, 2021, **273**, 118619.
39 G. M. Pontes-Quero, L. Benito-Garzón, J. Pérez Cano, M. R. Aguilar and B. Vázquez-Lasa, *Mater. Sci. Eng., C*, 2021, **121**, 111793.
40 C. Sánchez-Moreno, J. A. Larrauri and F. Saura-Calixto, *J. Sci. Food Agric.*, 1998, **76**, 270–276.
41 C. Pucci, C. Martinelli, D. De Pasquale, M. Battaglini, N. Di Leo, A. Degl'Innocenti, M. Belenli Gümüş, F. Drago and G. Ciofani, *ACS Appl. Mater. Interfaces*, 2022, **14**, 15927–15941.
42 T. C. P. Dinis, V. M. C. Madeira and L. M. Almeida, *Arch. Biochem. Biophys.*, 1994, **315**, 161–169.
43 N. Shenoy, M. Stenson, J. Lawson, J. Abeykoon, M. Patnaik, X. Wu and T. Witzig, *Lab. Investig.*, 2017, **97**, 494–497.
44 H. Kim and X. Xue, *J. Vis. Exp.*, 2020, **2020**, 1–5.
45 D. Fernández-Villa, G. Asensio, M. Silva, R. A. Ramírez-Jiménez, L. Saldaña, N. Vilaboa, A. Leite-Oliveira, J. San Román, B. Vázquez-Lasa and L. Rojo, *Eur. J. Med. Chem.*, 2021, **212**, 113152.
46 K. Wu, W. Hua, X. Li and J. Lin, *Chem. Eng. J.*, 2022, **446**, 136835.
47 J. Guo, Y. Ping, H. Ejima, K. Alt, M. Meissner, J. J. Richardson, Y. Yan, K. Peter, D. Von Elverfeldt, C. E. Hagemeyer and F. Caruso, *Angew. Chem., Int. Ed.*, 2014, **53**, 5546–5551.
48 J. Iglesias, E. García de Saldaña and J. A. Jaén, *Hyperfine Interact.*, 2001, **134**, 109–114.
49 J. D. Hem, *Water Supply Pap.*, 1960, **1459**, 75–94.
50 G. G. Costa, C. C. S. M. Brito, A. J. Terezo, A. P. Cardoso, E. Y. Ionashiro and A. B. de Siqueira, *Open Chem. J.*, 2018, **5**, 158–171.
51 G. Tondi and A. Petutschnigg, *Ind. Crops Prod.*, 2015, **65**, 422–428.
52 M. Taha, I. Khan and J. A. P. Coutinho, *J. Inorg. Biochem.*, 2016, **157**, 25–33.
53 P. Moreau, S. Colette-Maatouk, P. Vitorge, P. Gareil and P. E. Reiller, *Inorg. Chim. Acta*, 2015, **432**, 81–88.
54 Ż. Arciszewska, S. Gama, M. Kalinowska, G. Świderski, R. Świsłocka, E. Gołębiewska, M. Naumowicz, M. Worobiczuk, A. Cudowski, A. Pietryczuk, C. De Stefano, D. Milea, W. Lewandowski and B. Godlewska-żyłkiewicz, *Int. J. Mol. Sci.*, 2022, **23**(2), 888.
55 W. Liu, T. Wang, C. Yang, B. W. Darvell, J. Wu, K. Lin, J. Chang, H. Pan and W. W. Lu, *Osteoporos. Int.*, 2016, **27**, 93–104.
56 G. Di Pompo, M. Cortini, N. Baldini and S. Avnet, *Cancers*, 2021, **13**, 1–21.
57 F. Xiong, Z. Qin, H. Chen, Q. Lan, Z. Wang, N. Lan, Y. Yang, L. Zheng, J. Zhao and D. Kai, *J. Nanobiotechnol.*, 2020, **18**, 1–14.
58 S. Mathew, T. E. Abraham and Z. A. Zakaria, *J. Food Sci. Technol.*, 2015, **52**, 5790–5798.

59 W. Chariyarangsitham, S. Krungchanuchat, P. Khuemjun and C. Pilapong, *Arab. J. Chem.*, 2021, **14**, 103312.
60 Q. Yang, C. Zhao, J. Zhao and Y. Ye, *Pharm. Biol.*, 2017, **55**, 428–434.
61 G. K. B. Lopes, H. M. Schulman and M. Hermes-Lima, *Biochim. Biophys. Acta, Gen. Subj.*, 1999, **1472**, 142–152.
62 H. A. Kleinveld, A. J. G. Swaak, C. E. Hack and J. F. Koster, *Scand. J. Rheumatol.*, 1989, **18**, 341–352.
63 Q. Ru, Y. Li, W. Xie, Y. Ding, L. Chen, G. Xu, Y. Wu and F. Wang, *Bone Res.*, 2023, **11**, 12.
64 A. Szwed-Georgiou, P. Płociński, B. Kupikowska-Stobba, M. M. Urbaniak, P. Rusek-Wala, K. Szustakiewicz, P. Piszko, A. Krupa, M. Biernat, M. Gazińska, M. Kasprzak, K. Nawrotek, N. P. Mira and K. Rudnicka, *ACS Biomater. Sci. Eng.*, 2023, **9**, 5222–5254.
65 Y. Huang, Z. Du, P. Wei, F. Chen, B. Guan, Z. Zhao, X. Zhang, Q. Cai, J. Mao, H. Leng and X. Yang, *Chem. Eng. J.*, 2020, **397**, 125352.
66 Y. Wu, X. Li, Y. Sun, X. Tan, C. Wang, Z. Wang and L. Ye, *Bioact. Mater.*, 2023, **20**, 111–125.
67 S. Choi, H. S. Jo, H. Song, H. J. Kim, J. K. Oh, J. W. Cho, K. Park and S. E. Kim, *Nanomaterials*, 2021, **11**(7), 1812.
68 B. Taciak, M. Białasek, A. Braniewska, Z. Sas, P. Sawicka, Ł. Kiraga, T. Rygiel and M. Król, *PLoS One*, 2018, **13**, 1–13.
69 J. N. Sharma, A. Al-Omran and S. S. Parvathy, *Inflammopharmacology*, 2007, **15**, 252–259.
70 D. Fernández-Villa, R. A. Ramírez-Jiménez, I. Aranaz, N. Acosta, B. Vázquez-Lasa and L. Rojo, *Int. J. Mol. Sci.*, 2022, **23**, 10054.
71 H. Y. Kim, H. J. Jeong, N. R. Han, J. B. Jang and H. M. Kim, *J. Food Biochem.*, 2018, **42**, 1–10.
72 D. Song, J. Zhao, W. Deng, Y. Liao, X. Hong and J. Hou, *Biochem. Biophys. Res. Commun.*, 2018, **503**, 3078–3085.
73 V. Mouriño, J. P. Cattalini and A. R. Boccaccini, *J. R. Soc., Interface*, 2012, **9**, 401–419.
74 W. Qiao, D. Pan, Y. Zheng, S. Wu, X. Liu, Z. Chen, M. Wan, S. Feng, K. M. C. Cheung, K. W. K. Yeung and X. Cao, *Nat. Commun.*, 2022, **13**, 1–15.
75 M. Martin-Del-Campo, R. Rosales-Ibañez, K. Alvarado, J. G. Sampedro, C. A. Garcia-Sepulveda, S. Deb, J. San Román and L. Rojo, *Biomater. Sci.*, 2016, **4**, 1596–1604.
76 H. Hapidin, N. A. A. Romli and H. Abdullah, *Microsc. Res. Tech.*, 2019, **82**, 1928–1940.
77 H. Hapidin, N. M. Hashim, M. Z. Kasiram and H. Abdullah, *Molecules*, 2022, **27**, 451.
78 T. H. Pham, E. Kim, N. M. Trang and G. Jeong, *J. Periodontal Res.*, 2023, **59**, 204–219.
79 E. Torre, *Phytochem. Rev.*, 2017, **16**, 1183–1226.

